ARTICLE

Development of Local-Scale High-Resolution Atmospheric Dispersion Model Using Large-Eddy Simulation. Part 5: Detailed Simulation of Turbulent Flows and Plume Dispersion in an Actual Urban Area under Real Meteorological Conditions

Hiromasa Nakayama[a,*], Tetsuya Takemi[b], and Haruyasu Nagai[a]

[a] *Japan Atomic Energy Agency, 2-4, Shirakatashirane, Tokai-mura, Naka-gun, Ibaraki 319-1195, Japan;* [b] *Disaster Prevention Research Institute, Kyoto University, Kyoto, Japan*

(Received)

We have developed a LOcal-scale High-resolution atmospheric DIspersion Model using Large-Eddy Simulation (LOHDIM-LES) to assess the safety at nuclear facilities and to respond to emergency situations resulting from accidental or deliberate releases of radioactive materials (e.g., a terrorist attack in an urban area). In part 1-4, LESs of turbulent flows and plume dispersion over a flat terrain, around an isolated building, within building arrays with different obstacle densities, and within an actual urban area were performed, which showed the basic performance comparable to wind tunnel experimental technique. In this study, we extend the LOHDIM-LES to turbulent flows and plume dispersion in an actual urban area under real meteorological conditions by coupling with a meso-scale meteorological simulation model. The LES results of wind speed, wind direction, and concentration values are generally reproduced well. It is concluded that our coupling approach between LES and meso-scale meteorological models is effective in detailed simulations of turbulent flows and plume dispersion in urban areas under real meteorological conditions.

KEYWORDS: local-scale high-resolution atmospheric dispersion model, nuclear emergency response system, large-eddy simulation, meso-scale meteorological model, coupling simulation, turbulent flows, plume dispersion

*Corresponding author, E-mail: nakayama.hiromasa@jaea.go.jp

1. Introduction

There have been several serious nuclear accidents during the past 35 years: the Three Mile Island (1979, USA), Chernobyl (1986, USSR), and Fukushima (2011, Japan). In an emergency response to domestic nuclear accidents [1], the System for Prediction of Environmental Emergency Dose Information (SPEEDI) has been operated by the Japanese government. The SPEEDI was developed by Japan Atomic Energy Agency. This system consists of a meso-scale meteorological (MM) model and Lagrangian particle dispersion model, which can provide near real-time predictions of the mean air concentration and surface deposition of radionuclides in a regional scale of approximately 100×100 km^2 at several hundred meters of grid resolution. Hashimoto *et al*. [2] discussed the trade-off problem between computational cost and accuracy of MM models. First, they examined the sensitivity of three different grid resolutions (3 km, 1 km, and 333 m) and statistically evaluated the accuracy of MM models in comparison to the observations. Then, they showed that the improvement factors gradually become small in changing grid resolution from 1 km to 333 m although these models generally improve it with higher grid resolution. From these facts, they concluded that the upper limit of the MM simulation accuracy on grid resolution is observed and MM simulations at 333 m grid provide satisfactory results. This indicates that grid resolution of a few hundred meters in MM models is considered to be reasonable considering the trade-off problem. However, it is difficult to reproduce turbulent winds owing to the effects of urban obstacles or individual buildings within a nuclear facility that is not explicitly represented in meteorological models even at a fine grid resolution.

On the other hand, in local-scale atmospheric dispersion problems, an important issue is the accurate prediction of airborne radionuclides materials released from nuclear facilities for safety and consequence assessments. In distances of up to of several kilometers from the emission source, it is necessary to predict the air concentration fluctuations at the evaluation point for internal doses and surface concentration for external doses to evaluate the radiological consequences of the release of radioactive or toxic materials by taking into

account turbulent effects produced by individual roughness elements and terrain variability. Another issue is the potential problem of hazardous or flammable materials being accidentally or intentionally released in populated urban areas. In such a situation, it is important to predict possible spatial distributions of the contaminant plume, considering the arrangement and sizes of individual buildings and obstacles in the urban area. However, it is difficult to represent turbulent effects produced by building structures because these roughness elements cannot be explicitly resolved by a MM model with a grid resolution of several hundred meters.

For simulating turbulent winds and plume dispersion in a local-scale of several kilometers, there are typically two approaches: one is a wind tunnel experimental technique, and the other is a numerical simulation technique by computational fluid dynamics (CFD). It is well known that wind tunnel experiments are a rational tool for predicting plume dispersion behavior under local topography and/or building conditions. In the safety assessment for the construction of nuclear facilities in Japan, wind tunnel experiments of the spatial distribution of radionuclide concentrations over complex terrain containing buildings are required [3]. In the safety assessment, experimental results are used only to derive the effective stack height, which is applied for long-term assessment using a Gaussian plume model. The effective stack height is often found to be lower than the actual height of the stack, considering terrain and building effects in a way that provides a conservative evaluation to ensure that ground-level plume concentrations from the effective stack height do not fall below those from the actual one. Although reliable data on wind velocity and material concentrations can be obtained by a wind tunnel experiment, this approach has limited availability for these applications because wind tunnel testing is very expensive and time-consuming.

On the other hand, a numerical simulation technique using the CFD also has been recognized as a helpful tool. With the rapid development of computational technology, a CFD simulation technique has been evolving as an alternative to wind tunnel experiments. It numerically simulates airflow, heat transfer, and mass transfer by solving the governing equations. In principle, there are two different practically relevant approaches – the

Reynolds-Averaged Navier-Stokes (RANS) and the Large-Eddy Simulation (LES) models. RANS-based CFD models calculate a mean wind flow, delivering an ensemble- or time-averaged solution, and all turbulent motions are modeled using a turbulence model. The main advantage of the RANS model is its efficiency in computing a mean flow field with relatively low computational cost. Sada *et al*. [4] designed a RANS-based CFD model for simulating plume dispersion of radionuclides materials in nuclear facilities and showed favorable performance in comparison to wind tunnel experiments. Recently, LES-based CFD models have also come to be regarded as a useful tool. LES models resolve large-scale turbulent motions and model only small-scale motions. Although an LES model requires higher computational costs than a RANS model, it should be equally or more useful, considering the cost and limited availability of wind tunnels and the experimental time needed. Furthermore, LES models have potential performance to provide accurate data of turbulent flows and plume dispersion comparable to wind tunnel experiments. Therefore, we have developed the LOcal-scale High-resolution atmospheric DIspersion Model using Large-Eddy Simulation (LOHDIM-LES) and investigated the basic performance in comparison to wind tunnel experiments of turbulent flows and plume dispersion over a flat terrain and a two-dimensional hill, around an isolated building, within building arrays with different obstacle densities, and within a central district of an actual urban area [5]-[9].

However, our previous studies focus on turbulent flows and plume dispersion simulated by wind tunnel technique in which boundary layer flows represent idealized atmospheric motions and processes. Real atmospheric flows are composed of not only turbulence but also meteorological disturbances having various types of atmospheric motions with different time and spatial scales. According to a classification scheme for meteorological phenomena, atmospheric motion patterns can be divided into mainly two groups: micro-scale ranging from the order of 1 m to 10 km and meso-scale ranging from the order of 10 km to 100 km [10]. Micro-scale phenomena are characterized by wind shear and thermal stability, such as turbulence, building wake, thermal plumes, boundary layers, etc.

Meso-scale phenomena include thunderstorms, deep convection, urban heat island, land-sea breeze, orographic effects, meso-cyclones, fronts, etc. In producing micro- and meso-scale atmospheric phenomena by computational simulations, CFD and MM models are commonly used, respectively. In MM models, meteorological data such as surface pressure, wind velocity, temperature, relative humidity and geopotential height are used. Ground surface geometries are represented using terrain data on topography based on the terrain-following coordinate. These models typically use grid spacing between 1 km and several 10 km to resolve meso-scale phenomena. Aerodynamic characteristics of ground surfaces are usually represented as simplified parameterizations such as roughness-length and drag-force approaches. The values of roughness-length and drag coefficient are given depending on typically land-use with 24-categories. Although the accuracy of MM models for daily weather is continuously improving, it is difficult to reproduce wind fluctuations due to the effects of urban buildings that are not explicitly represented in these models. In CFD models, micro-scale atmospheric phenomena are reproduced by numerically calculating the basic equations of conservation of mass, momentum, and/or temperature. These models typically use grid spacing of the order of 1 m to capture small-scale turbulent flows. Therefore, an approach to couple a CFD model ~~between~~ with a MM model ~~and CFD models~~ should be promising to reproduce micro-scale flows under real meteorological conditions.

Recently, many researchers have studied about coupling technique. For example, Baklanov and Nuterman [11] proposed multi-scale systems for assessment and forecasting of urban meteorology, air pollution and emergency preparedness by coupling a CFD model with a NWP (numerical weather prediction) model. Tewari *et al*. [12] conducted micro-scale CFD simulations of plume dispersion in an urban area. In their coupling approach, initial and boundary conditions of the CFD model was determined by MM model outputs. They showed reasonable computed results in comparison to the field experimental data of averaged concentration values. Liu *et al*. [13] supplied lateral and top boundaries of the LES-based CFD model using MM outputs and estimated concentration of carbon monoxide over a

built-up urban district. Michioka *et al*. [14] also carried out LES-based CFD simulations of tracer gas dispersion in a real residential area coupled to a MM model, and compared simulation results to field experimental data. It was shown that the results of the CFD model combined with the MM model are significantly better than those not combined with the MM model. Wyszogrodzki *et al*. [15] also coupled an LES-based CFD model with a MM model and conducted detailed simulations of plume dispersion in a central district of an urban area. They mentioned that the calculated concentration footprints similar to the real ones are obtained in comparison to the field experiments. These studies imply that coupling simulations between MM and CFD models have a potential of becoming an effective tool to predict plume dispersion in a local-scale under real meteorological conditions. However, their focuses are mainly on a comparison of general distribution patterns of mean concentrations or scatter for statistic values of mean and peak concentrations. Actual urban surface geometries are very complex and highly inhomogeneous because the grounds are covered with many buildings with very variable sizes and heights. Lower part of atmospheric boundary layer called as roughness sub-layer is strongly influenced by the individual roughness obstacles, which brings about strong three-dimensionality of the flow. The transport process and unsteady behaviors of a plume are also expected to become highly complex. Therefore, in order to validate an LES-based CFD model, not only basic statistic values but also characteristics of concentration fluctuations should be investigated in detail. In this study, we extend the LOHDIM-LES to simulating real meteorological conditions by coupling with a MM model and investigate the basic performance in comparison to field experimental data of boundary layer flows and unsteady behaviors of plume dispersion in a central district of an actual urban area.

2. Approach to couple ~~between MM and~~ an LES-based CFD with a MM model ~~models~~

2.1. Numerical model

The LES-based CFD model used in this study is the LOHDIM-LES. The governing

equations are the filtered continuity equation, the Navier–Stokes equation, and the scalar conservation equation. The building effect is incorporated into the Navier–Stokes equation as an external force represented by the immersed boundary method proposed by Goldstein *et al*. [16]. The validity of this method was shown from the previous LES studies of complex turbulent flows in various surface geometries [6], [8], [9]. The subgrid-scale turbulent effect is represented by the standard Smagorinsky model [17] with a constant value of 0.1. The grid-filter width is given by $\overline{\Delta} = \left(\overline{\Delta}_x \overline{\Delta}_y \overline{\Delta}_z\right)^{\frac{1}{3}}$, where $\overline{\Delta}_x$, $\overline{\Delta}_y$, and $\overline{\Delta}_z$ are the grid spacing in the streamwise, spanwise, and vertical directions, respectively. Overbars ($\overline{\ }$) denote application of the spatial filter. The subgrid-scale scalar flux is also parameterized by an eddy viscosity model. The turbulent Schmidt number is set to 0.5 because this constant value is applicable to plume dispersion over a flat terrain [5], around an isolated building [6], over a two-dimensional hill [7], in building arrays with various obstacle densities [8], and within an actual urban area [9]. Information on the computational code such as the coupling algorithm of the velocity and pressure fields, the Poisson equation for pressure, and the spatial discretization in the basic equation is provided in part 1 - 4 of this paper series.

In the LOHDIM-LES, the approach to reproduce local-scale atmospheric flows is designed based on wind tunnel experimental technique. Thus, a long fetch parallel to a mean wind direction is set up at the upstream area of a main analysis region in order to drive turbulent inflows as shown in Fig. 1(A). In this driver region, first, a target mean wind flow is imposed at the inlet boundary and then, turbulent fluctuations produced by a recycling method proposed by Kataoka and Mizuno [18] and moderately setting up roughness obstacles are added to the inflow. The formulation of the recycling method is as follows:

Fig.1

$$u_{inlt}(y,z,t) = \langle u \rangle_{mean}(y,z,t) + \phi(z)\left\{u_{recy}(y,z,t) - [u](y,z)\right\} \quad (1)$$

$$v_{inlt}(y,z,t) = \langle v \rangle_{mean}(y,z,t) + \phi(z)\left\{v_{recy}(y,z,t) - [v](y,z)\right\} \quad (2)$$

$$w_{inlt}(y,z,t) = \langle w \rangle_{mean}(y,z,t) + \phi(z)\left\{w_{recy}(y,z,t) - [w](y,z)\right\} \quad (3)$$

Where u, v, and w are the wind components of the streamwise (x), spanwise (y), and vertical (z) directions, respectively. The suffixes of inlt, mean, and recy indicate the

instantaneous wind velocity at the inlet, the target mean wind velocity at the inlet, and the instantaneous wind velocity at the recycle station, respectively. [u], [v], and [w] are horizontally averaged winds over the driver domain and $\phi(z)$ is a damping function. It was shown that this approach can successfully produce various types of wind tunnel flows. In the previous study, we applied the recycling technique to coupling between MM and LOHDIM-LES, and conducted test simulations of strong winds over an actual urban central district during the passage of a major typhoon [19]. In this calculation, $\langle u \rangle_{mean}$, $\langle v \rangle_{mean}$, and $\langle w \rangle_{mean}$ of Equations (1)-(3) were given by the MM wind velocities calculated based on RANS simulations. It was shown that the observed ranges of wind fluctuations and gust factors were reasonably reproduced in comparison to the observed data (see Figs. 4 and 6 in the paper of Nakayama *et al*. [19]). This fact indicates that time-dependent turbulent inflow data can be effectively generated from mean wind velocities of a MM model by using the recycling technique.

However, mean wind directions are not always constant and often vary due to a change of weather conditions. Therefore, a long fetch type of computational models parallel to mean wind directions have a limitation for a case of largely varying mean wind directions. In this study, we improve inflow boundary conditions in order to automatically input wind velocity data with spatially-varying mean wind directions obtained by a MM model into the LOHDIM-LES.

2.2. Improvement of inflow boundary conditions

In coupling a LES-based CFD model with a MM model, time-dependent turbulent inflow data should be imposed at the inlet boundary. Several approaches to couple ~~between MM and~~ an LES-based CFD model with a MM model ~~models~~ have recently been demonstrated to produce micro-scale flows under real meteorological conditions. For example, Wyszogrodzki *et al*. [15] coupled an LES-based CFD model with a MM model to conduct detailed simulations of plume dispersion in an urban central district, considering

meteorological effects. They set up five nested MM computational domains which cover 4050 km, 1350 km, 450 km, 150 km, and 45 km square areas with 40.5 km, 13.5 km, 4.5 km, 1.5km, and 0.5 km grid resolutions, respectively, and one LES-based CFD model covering an area of 1.79 km × 1.79 km with 4 m grid. In the downscale data transfer, they set up high-resolution grid for the vertical direction in the MM model in order to reproduce basic flow characteristics within a planetary boundary layer. The MM outputs such pressure, velocity, and potential temperature calculated based on RANS simulations are directly imposed at the inflow boundaries of the LES-based CFD model. Although they provided reasonable results in comparison to field experimental data of mean and peak concentrations, those MM outputs do not include high-frequency turbulent fluctuations appropriate to drive LES-based CFD models. Michioka *et al*. [14] coupled an LES-based CFD model with LES-based MM models for detailed simulations of plume dispersion in a residential area under real meteorological conditions. They set up six nested MM computational domains which cover 1944 km, 648 km, 216 km, 72 km, 24 km, and 8 km square areas with 24.3 km, 8.1 km, 2.7 km, 0.9 km, 0.3 km, and 0.1 km grids, respectively, and one LES-based CFD computational domain which covers an area of 2 km × 2 km with horizontally stretched grid resolution ranging from 1.5 m to 40 m. Turbulent fluctuations are generated by gradually downscaling the LES-based MM models and are imposed at the inflow lateral boundaries of the LES-based CFD model. Although small-scale wind fluctuations under real meteorological conditions are appropriately reproduced to drive an LES-based CFD model, their approach requires substantial computational time and resource for many nested simulations of MM models.

In contrast to these approaches, in which MM simulations are improved, we propose a new scheme to treat boundary conditions of LES-based CFD model for coupling simulations using a turbulent inflow technique. Two nested domains are set for LES-based CFD simulation as shown in Fig. 1(B). The main analysis domain is located at the center part of the square shaped outer domain that has the same role as the driver region of LOHDIM-LES in

Fig. 1(A). In the outer domain, a target mean wind flow with turbulent fluctuations is reproduced by using MM outputs. First, mean wind directions in a MM model are estimated and vertical planes of inflow boundaries are automatically determined depending on them. For example, when mean wind directions of a MM model θ range from -315° to 0° or from 0° to 45° , vertical boundary planes in the west, north, and east sides are automatically set to inflow boundaries and that in the south side is set to an outflow boundary. In cases of θ ranging from 45° to 135° , from 135° to 225° , and from 225° to 315° , the method to determine inflow and outflow boundaries depending on θ is shown in Table 1. Then, turbulent fluctuations generated by the recycling method are added to the MM outputs at the inflow boundaries. The method to set up turbulent inflow boundaries depending on θ is also shown in Table 1.

Tab.1

In this study, a nudging term is also incorporated into the Navier–Stokes equation in order to maintain the structure of mean flow produced by the MM model in the LES-based CFD domain, and is expressed by the following expression;

$$F_{nud,i} = -\alpha\left(u_{MM,i} - u_i\right) \tag{4}$$

where α is a spatially dependent nudging constant (see details for the specification of α in section 3.3) and $u_{MM,i}$ is i-component of wind velocity of a MM model based on ensemble-averaged turbulence models. A nudging constant is set to rapidly vary from 0.0 s^{-1} to 0.01 s^{-1} across 750 m height using a hyperbolic tangent function and decrease from the lateral boundaries toward the inner part using a ten-grid-point buffer zone. In real meteorological fields, mean wind directions are often largely different between upper and lower parts of boundary layers, which tended to lose the balance between inflow and outflow and often induces numerical instabilities in our test simulations. Therefore, in case spatially-averaged wind directions at heights less than 750 m differ from those above it by 30 degrees at the main inlet boundary, each component of wind velocities at heights greater than 750 m are set to that at height of 750 m. By these procedures, the flow rate is balanced at the boundaries.

The treatment of the nudging procedure requires some cautions. For example, Moeng and Rotunno [20] conducted LES numerical experiments of buoyancy-driven turbulent flows and reported that the turbulent structures of convective boundary layers are sensitively influenced by the treatment of the top boundary conditions. For a case the top boundary is set to no-slip condition, most of the impinging updrafts lose their kinetic energy to the viscous dissipation, and only weak and broadly distributed returning downdrafts exist among the updrafts. Thus, the skewness of the vertical velocity (S_w) increases with height and reaches a maximum right beneath the no-slip top. On the other hand, for a case the top boundary is set to free-slip condition, there is no viscous dissipation at the free-slip wall, and the S_w remains relative constant there. Sullivan *et al*. [21] also showed that the inversion height is variable depending on the temperature jump around the inversion height and influenced by the grid resolution. They mentioned that the coarse-mesh simulation generally predicts a value of the inversion height greater than its fine-mesh counterpart at the same dimensionless time. These studies imply that the nudging procedure should be carefully used in order to accurately capture vertical turbulent motions across the inversion height depending on the meteorological conditions. However, our focus is on plume dispersion near a ground surface. Therefore, the influence of the nudging procedure is considered to be negligible.

3. Test Simulations

3.1. Dataset of the Field Experiments for Estimating Prediction Accuracy [22]

The field experiments of Joint Urban 2003 were conducted in the central district of Oklahoma City from June 28 through July 31, 2003 by a large number of organizations such as the U.S. government institutes, U.S. universities, other U.S. federal agencies and private companies. The focus of this field campaign is to better understand atmospheric dispersion process of a tracer gas in urban environments under varying atmospheric conditions. Therefore, many model researchers used the detailed meteorological and concentration data for model evaluation study (Wyszogrodzki *et al*. [15], Warner *et al*. [23], Chan and Leach [24],

Hendricks *et al*. [25], and Hanna *et al*. [26]).

In these experiments, wind velocities were measured by meteorological instruments such as lidars, sodars, radars, and sonic anemometers in and around the central district. Sulfur hexafluoride (SF_6) tracer was released as puffs and 30-minute continuous releases from one of three release locations during the 10 main IOPs (intensive observation periods). The first six IOPs and the last four ones were conducted in the daytime and the nighttime, respectively. During each IOP, typically three 30-minute continuous and four instantaneous releases from a ground-level were conducted. The release conditions are given in Table 2.

Tab.2

The cases studied here are the events of the first three 30-minute continuous plume release from the Botanical garden at 0900, 1100, and 1300 Central Daylight Time (CDT) in IOP6. In this study, we used the data of vertical profiles of wind speed and directions obtained at the three points A, B, and C which are located 1.8 km south-southwest from the Botanical garden, in the garden, and 1.6 km north from the garden, respectively, as shown in Fig. 2. Those obtained at the point A were measured by sodar (Pacific Northwest National Laboratory), and those at the points B and C were measured by minisodar (Argonne National Laboratory). In order to investigate prediction accuracy of unsteady behaviors of plume dispersion simulated by the LOHDIM-LES in detail, we used the concentration data measured by fast-response tracer analyzers with a time response of approximately 1 Hz by Lawrence Livermore National Laboratory (LLNL). These analyzers were set at eight points mainly above Robinson Avenue and Sheridan Avenue located within two hundred meters downstream of a point source. The release location and measuring points are shown in Fig. 3. In our previous study, it was shown that the spatial extent of concentration distribution patterns significantly influenced by urban surface geometries is a few hundred meters from a point source (Nakayama *et al*. [27]). By comparing with the experimental data of the high-frequency concentration fluctuations measured in the very short-range, we estimate prediction accuracy for the area where individual urban buildings largely influence the formation of plume concentration distributions.

Fig.2

Fig.3

3.2. Meso-scale meteorological model (MM)

The model used for a MM simulation is the Weather Research and Forecasting (WRF) model, the Advanced Research WRF Version 3.3.1 (Skamarock *et al*. [28]). We use a nesting capability to resolve the Oklahoma City region at a fine grid spacing by setting two-way nested, three computational domains (with the top being at the 50-hPa level). The three domains cover 2700 km, 600 km, and 150 km square areas with 4.5 km, 1.5 km, and 0.5 km grids, respectively, as shown in Fig. 4 (a)-(c). The number of vertical levels is 53, with 12 levels in the lowest 1-km depth.

Fig. 4

The terrain data used are the global 30-second data (GTOPO30) from the U.S. Geological Survey (USGS). The land-use/land-cover information is determined by the 30-second resolution Global Land Cover Characterization dataset. To determine the initial and boundary conditions for the atmospheric and surface variables, we use 6-hourly Final Analysis (FNL) data of the U.S. National Centers for Environmental Prediction (NCEP). The horizontal resolution of NCEP FNL data is 1 degree. Full physics processes are included in the present simulation in order to reproduce real meteorological phenomena. A physics parameterization closely relevant to the simulation of wind fields is a planetary boundary layer (PBL) mixing parameterization. We choose a Mellor-Yamada Level 2.5 scheme of Janjic [30] in which mixing is done vertically between the adjacent vertical levels. A single-moment, 6-category water- and ice-phase microphysics scheme is employed for cloud and precipitation processes in all the domains. No cumulus parameterization is used for all the domains. In representing aerodynamic characteristics of ground surfaces, roughness-length approach is usually used. The roughness length z_0 is automatically determined by the USGS 24-category land-use data. For example, the value of z_0 is 0.8 m for urban areas. In order to simulate the atmospheric conditions of IOP6, the simulated period is from 1900 CDT 14 July to 1900 CDT 16 July 2003. The nested inner domains are initialized at 1900 CDT 15 July for the first inner domain and at 0700 CDT July 16 for the second inner domain. The WRF

simulated outputs of the innermost domain at 1-minute interval are used as the inputs of an LES model.

3.3. Calculation conditions of LES-based CFD model

In the LOHDIM-LES, buildings and structures in the central district of Oklahoma City are explicitly represented by the use of a digital surface model dataset [30]. The model is configured using two nested domains with one-way interaction between outer and inner domains as shown in Fig. 4 (d)-(e). The outer and inner domains cover areas of 8 km by 8 km by 1.5 km with the grid spacing of 20 m by 20 m by 2-20 m stretched and 1.6 km by 1.6 km by 0.75 km with the grid spacing of 4 m by 4 m by 2-20 m stretched in the streamwise, spanwise and vertical directions as shown in Fig. 5(a) and (b), respectively. The validity of this model set-up was examined in comparison to the observed and wind tunnel experimental data from the previous LES studies [9], [19]. In both domains, roughness blocks are placed around the central district to maintain urban boundary layer flows throughout the computational domains.

Fig. 5

In the outer domain, MM outputs and turbulent fluctuations generated by a recycling technique are imposed at the main inlet boundary as described in section 2. The boundary conditions at the outflow planes are: a Sommerfeld radiation condition (Gresho [31]) at the outflow boundary; a free-slip condition for the horizontal velocity components and zero-speed condition for the vertical velocity component at the upper boundary; a no-slip condition for each velocity component at the bottom surface. However, the surface grid spacing of 2.0 m in the vertical direction is coarse for the no-slip boundary condition. In future work, we need to incorporate wall functions into our LES model. The time step interval Δt is 0.1-second. The inlet and spanwise boundaries are determined by the WRF outputs (with 1-minute interval and 500 m resolution) linearly interpolated on the grids of the outer domain with 1-minute interval. In the inner domain, the time step interval Δt is 0.02-second. The inlet and spanwise boundaries are determined by the outputs of the outer domain linearly interpolated

on the grids of the inner domain with 0.1-second interval. The nudging procedure is applied only at the lateral boundaries using a ten-grid-point buffer zone.

In our LES models, a neutral atmospheric stability condition is assumed, which requires some cautions. Moeng and Sullivan [32] conducted LESs of neutrally- and unstably-stratified boundary layers and investigated the difference of the turbulent structures. They reported that streaky structures are formed near the wall for the shear dominated flow case and strong updrafts that are roughly comparable to the boundary layer scale are observed for the buoyance dominated flow case. This indicates that turbulence structures in neutral and unstable conditions are essentially different. On the other hand, Lundquist and Chan [33] conducted CFD simulations of turbulent flows in an urban area for the nighttime and daytime, and quantitatively investigated the influence of building-induced turbulence and buoyant forcing from turbulence kinetic energy (TKE) budget inside and outside of the urban area. They reported that the contribution of the buoyancy to the total TKE is negligible for the night time and buoyancy production contributes approximately 25% of the total TKE within the urban area. This indicates that the building-induced turbulence is the dominant source of TKE within the urban area. Furthermore, Lundquist *et al*. [34] conducted LESs of plume dispersion in the urban central district under the assumption of a neutral stability and showed reasonable results in comparison to the field experimental data. From these facts, they concluded that the assumption of a neutral stability is valid for within an urban area where building-induced turbulence is dominant. However, it should be noted that the assumption is less valid for the urban wake region because the levels of building-induced turbulence greatly subside [33]. Although our approach based on the assumption of a neutral stability doesn't produce the exact same turbulence structure as that of the thermally developing PBL, it is valid for simulation of plume release within an urban area where building-induced turbulence is dominant.

The three calculation cases for the events of three 30-minute continuous plume release are separately carried out. In the outer domains, the simulation periods are from 0700 to 0940,

from 0900 to 1140, and from 1100 to 1340 for cases1, 2, and 3, respectively. The simulation periods of the inner domains are from 0800 to 0940, from 1000 to 1140, and from 1200 to 1340 for cases1, 2, and 3, respectively. The beginning and ending time of plume release are set to the same as that of the field experiment as shown in Table 3.

4. Results

4.1. Flow Field

Figure 6 shows instantaneous shot of turbulent flows in the outer and inner domains of the LOHDIM-LES. It is found that urban boundary layer flows are generated by the recycling method using the WRF outputs and small-scale turbulent flows in the urban central district are produced by downscaling from the LES outer domain. Fig. 6

Figure 7 shows time series of wind speeds of the observed, WRF, and LES data at heights of 100 m, 200 m, and 300 m at the point A in the LES outer domain for each case. Wind speeds of the WRF at 100 m height are generally similar to the observed data except time period from 13:45 to 14:00 in the cases2 and 3. With the development of daytime convective boundary layer, the WRF data vary more actively in the cases2 and 3 while those are nearly constant in the case1. The LES instantaneous values generally fluctuate around the WRF data at each height for each case although the magnitude of the wind fluctuations comparatively becomes small for the cases2 and 3. The difference between the observed and LES data are due to the calculation errors of the WRF model. Fig. 7

Figure 8 compares power spectra of wind velocity fluctuations of the LES at heights of 10m, 100 m, 200 m, and 300 m with those of Karman type. ~~Here, f, $E(f)$, σ_u, and L_{ux} are frequency, streamwise velocity spectrum, standard deviation of streamwise velocity fluctuations, and integral length scale, respectively. Although power spectra of the LES rapidly decrease on the higher-frequency side because of the comparatively small turbulent fluctuations especially for the cases2 and 3, the LES data are generally in agreement with the Karman type around the peak frequency $fL_{ux}/U = 0.12$ at each height for each case.~~ Here, f, $E(f)$, σ_u, σ_v, L_{ux} Fig. 8

and L_{vx} are frequency, spectrum, standard deviation of streamwise and spanwise velocity fluctuations, and streamwise and spanwise integral length scale, respectively. The power spectra of the LES rapidly decrease on the higher-frequency side and are not distributed along the Karman type especially at heights of 100m - 300m for cases 2 and 3, which indicates that the inertial subrange is not fully represented. However, those of the LES at 10m height are generally distributed along those of the Karman type on the higher-frequency side.

Figures 9-14 show vertical profiles of wind speeds and wind directions of the experiments, WRF, and LES obtained at the points A, B, and C for cases1, 2, and 3. In the case1, vertical profiles of the WRF wind speeds and wind directions generally show good agreements with the experimental data at the points A and C. However, at the point B, wind speeds of the WRF are generally overestimated at each measuring time. Wind directions of the WRF are also nearly homogeneous in the vertical direction at each measuring time while the experimental data rapidly vary from the ground surface to a few dozens of meters due to roughness elements such as buildings and trees in the Botanical garden. In the cases2 and 3, wind speeds of the WRF become nearly homogeneous in the vertical direction due to daytime convective development at each point while local variations and rapid increase of wind speeds and wind directions of the experiments are still occasionally observed at the lower part of the boundary layer especially at the point B.

Figs. 9-14

As described in part 4 of this series, building height variability V_h and building frontal area index λ_f for the central district of Oklahoma City is 1.0 [-] and 0.15 [-], respectively. Here, the values of V_h and λ_f are defined as the ratio of standard deviation of building height to average building height and the ratio of total frontal area of roughness elements to total surface area. Roughness length is an important parameter and is commonly used to describe surface aerodynamic characteristics in meso-scale meteorological simulation models. From the LES analysis on the relationship between aerodynamic roughness parameters and building morphological characteristics (Nakayama *et al.* [35]), it was suggested that defining roughness length values become more difficult for larger $\lambda_f > 0.16$

and V_h > 0.5, and the influence of higher buildings on boundary layer structure becomes significantly large. Although the λ_f value is slightly smaller than the range, it is difficult to reproduce winds at a ground level by conventional roughness length approaches because of the large V_h value. Urban effects should be appropriately incorporated into them by taking into account both densities and heights of roughness obstacles that represent real building configurations in order to accurately produce urban boundary layer flows near a ground surface. Although important issues remain in accurately reproducing urban boundary layers over ground surfaces covered with buildings with highly variable heights by the roughness length approach, the distribution patterns of wind speeds and directions are generally similar to the observed data. Therefore, it is considered that meteorological simulation data to impose at the LES inlet boundary conditions are reasonably reproduced.

Compared to the WRF data, there are differences between the WRF and LES data especially for the cases2 and 3 which correspond to well-developed daytime convective. These differences are because the present LES calculations are carried out under neutral conditions. The thermal effects should be incorporated into our LES model. However, the LES data of wind speeds and wind directions generally seem to fluctuate around them at each measuring point, which indicates that well-developed turbulent fluctuations are produced and the structure of mean flow is maintained. The difference between the experimental and LES data is mainly caused by the inaccuracy by the WRF model because the meteorological simulation data are used as the LES inflow boundaries. It is considered that our coupling approach between MM and LES-based CFD models reasonably reproduces small-scale turbulent flows under real meteorological conditions.

4.2. Dispersion field

4.2.1 Mean and fluctuating concentrations

Figure 15 shows instantaneous dispersion fields at 8-minutes after the plume release for each LES case. Instantaneous concentrations are normalized by the initial concentration

Fig. 15

C_{init} . In case1, the plume released from a continuously emitting point source at the upstream position of the central district is rapidly dispersed in the lateral direction due to the effect of individual urban buildings. From the influence of the mean wind direction in the meteorological field, the concentration distributions are generally formed toward the northeast direction. Furthermore, the high concentration regions of the plume are found to transport into Robinson Avenue and then the street behind the downtown hotel. In case2, the plume is generally dispersed in the south direction. The high concentration regions are mainly formed along Robinson Avenue and a part of the plume is transported into the west area of the Avenue. Also in case3, the plume is generally dispersed in the south direction and the high concentration regions are mainly formed along Robinson Avenue.

Figures 16-18 compare time series of concentrations fluctuations of the LES with the field experimental data for cases1, 2, and 3. Time-averaged concentration C_{ave} is estimated by the following procedure;

Figs. 16-18

$$C_{ave} = \frac{1}{T}\int_0^T c(t)\,dt \tag{5}$$

where c is instantaneous concentration and averaging time T is set to 30 minute corresponding to the continues release duration time. In the experiment case1, the averaged concentrations are relatively high at the points C, D and E, and intermediately high at the points, B, F, and H among the experimental values. At these points, instantaneous sharp high peak concentrations intermittently occur. At the points A and G, the occurrences of concentrations are less frequent and the averaged concentrations are also considerably low. These areas are considered to correspond to the edge of the plume. These experimental results imply that the plume is actively meandering around a point source and transported into Robinson Street and Sheridan Street. In the LES case1, the averaged concentrations are relatively high at the points C, D, G, and H, intermediately high at the point E, and considerably low at the points A, B, and F among the calculated values, which indicates that

the plume is mainly transported into the north side of Robinson Street and a part of the plume is dispersed toward the east side of Sheridan Street.

In the experiment case2, at the points C and D, the averaged concentrations are relatively high and instantaneous high concentrations frequently occur. At the points B and E the averaged concentrations are also relatively high and the concentration fluctuations are intermittent. At the points A, F, and H the averaged values are intermediately high and the concentration fluctuations are intermittent. At the point G, the averaged value is considerably low. It is found from these results that the plume is mainly transported toward the north of Robinson Street with active meandering motions. In the experiment case3, the tendencies of the distributions of the averaged concentration values and fluctuating patterns of concentrations depending on the measurement locations are similar to those for the case2. In the LES case2, the averaged concentrations are relatively high at the points C and H, intermediately high at the points A, B, D, and G, and considerably low at the points E and F among the calculated values. The LES results indicate that the plume is mainly transported into the north side of Robinson Street. In the LES case3, these tendencies depending on the measurement locations are similar to those for the case2.

It is found that there are significant differences of averaged and maximum concentrations of a plume at several positions between the field experiments and the LES model. This is due to the prediction errors of meteorological simulation data used to impose at the inlet boundary of the LES model. Furthermore, the frequencies of occurrences of concentrations are overestimated especially near the plume source due to numerical diffusion by a coarse grid resolution. According to a schematic diagram of plume dispersion in a real atmosphere shown by Davidson *et al*. [36], close to the point source, a plume spreads through small-scale turbulent mixing and meanders by the comparatively larger scale of turbulent eddies than the scale of a plume. The source point is represented by one grid with 4 m × 4 m in the LES model while the real diameter of the point source is 1 cm order in the field experiment. Michioka *et al*. [37] also mentioned that grid resolution for a point source

significantly influences on short-range concentration distributions of a plume from LES numerical experiments of the sensitivity of grid resolution for a point source corresponding to 1.0 and 10 times the real diameters of the one. Therefore, the overestimation of the frequencies of occurrences of concentrations is due to numerical diffusion by a coarse grid resolution for a point source.

4.3. Estimation of prediction accuracy

In order to investigate prediction accuracy in detail, scatter plot of various parameters such as arrival time, leaving time, duration time, intermittency, time-averaged concentration, and maximum concentration are estimated. The definition of the averaged value is described in the previous section. The maximum concentration $C_{\max}$ is defined as the maximum value during the 30 minute from the plume release start time to the end time. Intermittency is defined as the proportion of time for which $c > 0.05 \times C_{\max}$ during the 30 minute. The arrival and leaving time are defined as the time interval after the plume release when 5% and 95% of the total dosage of a plume reaches the measurement location as shown in Fig. 19. These definitions are based on the statistical study of puff dispersion by Harms *et al*. [38]. The duration time is defined as the difference between the arrival and leaving time. Scatter plot of these parameters are shown in Fig. 20.

Fig.19

Fig.20

In the LES model, the values of arrival time are overestimated especially for the cases2 and 3 at the points E and F that correspond to the areas where the plume is actively meandering in the experiment, and underestimated for the cases1 and 2 at the point D near the point source. Although the values of arrival time are considerably scattered for several points, those of leaving time are unexpectedly in good agreement with the experimental data for each case. As a result, those of duration time are considerably overestimated at the point D for the cases1 and 2, and underestimated at the points E and F for the cases2 and 3. The intermittencies of the LES model are highly overestimated at the several points due to numerical diffusion. The averaged concentrations are overestimated especially at the points C,

H, and G that correspond to the high concentration regions for each case, and underestimated especially at the points E and F that correspond to the areas where the plume is actively meandering in the experiments. The values of the maximum concentration are similar to the experimental values for the points at which the LES averaged values are comparable to the experimental ones.

From these facts, it is found that slight calculation errors in wind speeds and wind directions bring about significant differences of mean and fluctuating characteristics of a plume between the experiments and the LES model. Although the MM simulation data to impose at the LES inlet boundary conditions are reasonably reproduced, urban turbulent effects should be appropriately incorporated into the MM model in order to accurately reproduce wind velocities at a ground level. However, the LES model generally simulates the basic spatial distribution patterns of a plume and the fluctuating patterns of concentrations depending on measurement locations are similar to those of the experiments. Our LES model is considered to show high potential to provide detailed information on spatial extent of contaminated areas and plume dispersion behaviors in a local-scale under real meteorological conditions.

5. Conclusion

In this study, we extended the applicability of LOHDIM-LES to turbulent flows and plume dispersion in an actual urban area under real meteorological conditions. A new scheme to couple ~~between MM and~~ an LES-based CFD model with a MM model ~~models~~ was developed by using a recycling technique, and prediction accuracy of the extended LOADIM-LES was investigated in comparison to field experimental data. The obtained results are as follows:

1. The new method properly ingested time-dependent turbulent inflows from MM simulation data into an LES-based CFD model in order to simulate plume dispersion in a central district of an actual urban area under real meteorological conditions. The LES data

of wind speeds and wind directions seem to fluctuate around the MM data at each measuring point. This indicates that well-developed turbulent fluctuations are reproduced and the structure of mean flow is maintained. However, differences between the WRF and LES data are observed for a case of well-developed daytime convective boundary layer. These are because the present LES calculations are carried out under neutral conditions. The thermal effects should be incorporated into our LES model in a future work. Furthermore, the power spectra of the LES rapidly decrease on the higher-frequency side and are not distributed along the Karman type especially at heights of 100m - 300m during some period of time. Our coupling approach needs to be improved in order to reproduce more realistic turbulent fluctuations under real meteorological conditions. However, those of the LES at 10m height are generally distributed along those of the Karman type, which indicate that the dispersion behaviors of a plume released from a ground-level are considered to physically simulate.

2. Slight calculation errors in wind speeds and directions bring about significant differences of concentration values of a plume between the field experiments and our LES model at several positions. In order to accurately reproduce wind velocities at a ground level, urban turbulent effects should be appropriately incorporated into a MM model. Frequencies of occurrences of concentrations are overestimated especially near the plume source. This is because meandering motions are not reproduced well due to numerical diffusion by a coarse grid for a point source. However, the fluctuating patterns of concentrations depending on measurement locations are similar to the experimental data.
3. Although important issues remain in accurately reproducing transport and dispersion process of a plume, the LES model generally simulates the basic spatial distribution patterns of a plume. It can be concluded that our LES model have high potential to provide detailed information on spatial extent of contaminated areas and plume dispersion behaviors in a local-scale under real meteorological conditions.

In the previous studies [5]-[9], we showed that the LOHDIM-LES can simulate

various wind tunnel flows and plume dispersion behaviors by comparing wind velocities and mean and fluctuating concentrations between simulations and wind tunnel experimental data. In this study, we extend the LOHDIM-LES to simulating real meteorological conditions by coupling with a MM model. This coupling approach using a turbulent inflow technique can effectively reproduce time-dependent turbulent inflow data for LES models from mean wind field simulated by MM model. However, the current coupling calculation is designed based on the assumption of a neutral atmospheric stability. Because this assumption is less valid for the downwind regions of built-up areas, the coupling simulation should be carefully applied depending on the surface geometry type of the investigated site.

As another effective use, our coupling approach using a turbulent inflow technique indicates that wind field derived from vertical profile of meteorological observation by assuming horizontal homogeneity can be used as the input for the LOHDIM-LES. Tewari *et al*. [12] compared the performance of the following two different approaches of supplying initial and boundary conditions to drive the CFD model: (1) using stationery observed data and (2) using MM outputs. Although they reported that the approach of using MM outputs show higher performance from the standard statistical analysis of concentration values for short-range up to 2 km from the point source, the approach of using observations shows reasonable performance depending on the range of the investigated site. It is considered from these facts that the approach of using observations still has potential to drive CFD models for detailed estimation under real meteorological conditions.

Therefore, the current version of LOHDIM-LES has broad utility, i.e., simulations of wind tunnel experiment, real meteorological conditions based on MM simulations or observations, which are applicable to not only safety assessment of nuclear facilities as an alternative to wind tunnel experiments but also detailed simulations of plume dispersion in a local-scale in cases of nuclear accidents or urban dispersion by nuclear, biological, and chemical (NBC) agent terrorist attack.

References

[1] Nagai H, Chino M, Yamazawa H. [Development of scheme for predicting atmospheric dispersion of radionuclides during nuclear emergency by using atmospheric dynamic model], Trans. At. Energy Soc. Jpn. 1999; 41: 7: 777-785 [in Japanese].

[2] Hashimoto A, Ohsawa T, Yasuda T. Accuracy of the wind calculation over complex terrain with the meso-scale model MM5 and the higher limit of the horizontal resolution, J. Wind Eng. 2005; 30: 3: 65-74 [in Japanese].

[3] Meteorological Guide for Safety Analysis of Nuclear Power Plant Reactor. Nuclear Safety Commission of Japan. 1982.

[4] Sada K, Komiyama S, Michioka T, Ichikawa Y. [Numerical model for atmospheric diffusion analysis and evaluation of effective dose for safety analysis], Trans. At. Energy Soc. Jpn. 2009; 8: 184-196 [in Japanese].

[5] Nakayama H, Nagai H. Development of local-scale high-resolution atmospheric dispersion model using large-eddy simulation part1: turbulent flow and plume dispersion over a flat terrain, J. Nucl. Sci. Technol. 2009; 46: 1170-1177.

[6] Nakayama H, Nagai H. Development of local-scale high-resolution atmospheric dispersion model using large-eddy simulation part2: turbulent flow and plume dispersion around a cubical building, J. Nucl. Sci. Technol. 2011; 48: 374-383.

[7] Nakayama H, Nagai H. Large-Eddy Simulation on turbulent flow and plume dispersion over a 2-dimensional hill, Adv. Sci. Res. 2010; 4: 71-76.

[8] Nakayama H, Jurcakova K, Nagai H. Development of local-scale high-resolution atmospheric dispersion model using large-eddy simulation part3: turbulent flow and plume dispersion in building arrays, J. Nucl. Sci. Technol. 2013; 50: 503-519.

[9] Nakayama H, Leitl B, Harms F, Nagai H. Development of local-scale high-resolution atmospheric dispersion model using large-eddy simulation part4: turbulent flows and plume dispersion in an actual urban area, J. Nucl. Sci. Technol. 2014; 51: 626-638.

[10] Stull R. B. An introduction to boundary layer meteorology, Kluwer Academic. 1988: 20 pp.

[11] Baklanov A A, Nuterman R B. Multi-scale atmospheric environment modeling for urban areas, Adv. Sci. Res., 3, 53-57, 2009.

[12] Tewari M, Kusaka H, Chen F, Coirier W J, Kim S, Wyszogrodzki A, Warner T. Impact of coupling a microscale computational fluid dynamics model with a mesoscale model on urban scale contaminant transport and dispersion, Atmos Res. 2010; 96: 656-664.

[13] Liu Y S, Miao S G, Zhang C L, Cui G X, Zhang Z S. Study on micro-atmospheric environment by coupling large eddy simulation with mesoscale model, J. Wind Eng. Indus. Aerodyn. 2012; 107-108: 106-117.

[14] Michioka T, Sato A, Sada K. Large-eddy simulation coupled to meso-scale meteorological model for gas dispersion in an urban district, Atmos. Environ. 2013; 75: 153-162.

[15] Wyszogrodzki A, Miao S, Chen F. Evaluation of the coupling between mesoscale-WRF and LES-EULAG models for simulating fine-scale urban dispersion, Atmos Res. 2012; 118: 324-345.

[16] Goldstein D, Handler R, Sirovich L. Modeling a no-slip flow boundary with an external force field, J. Comput. Phys. 1993; 105: 354-366.

[17] Smagorinsky J. General circulation experiments with the primitive equations, Monthly Weather Review. 1963; 91: 99-164.

[18] Kataoka H, Mizuno M. Numerical flow computation around aeroelastic 3D square cylinder using inflow turbulence, Wind and Struct. 2002: 5: 379-392.

[19] Nakayama H, Takemi T, Nagai H. Large-eddy simulation of urban boundary-layer flows by generating turbulent inflows from mesoscale meteorological simulations, Atmos. Sci. Lett. 2012; 13: 180–186.

[20] Moeng C H, Rotunno R. Vertical-velocity skewness in the buoyancy-driven boundary layer. J. Atmos. Sci. 1990; 47: 1149-1162.

[21] Sullivan P P, Moeng C H, Stevens B, Lenschow D H, Mayor S D. Structure of the entrainment zone capping the convective atmospheric boundary layer. J. Atmos. Sci. 1998; 55: 3042-3064.

[22] Allwine K J, Flaherty J E. Joint Urban 2003 study overview and instrument locations. PNNL-15967, Pacific Northwest National Laboratory, Richland, WA, 2003.

[23] Warner S, Platt N, Jeffry T, Heagy J F. Comparisons of Transport and Dispersion Model Predictions of the Joint Urban 2003 Field Experiment. J. Appl. Meteor. Climatol., 2008; 47: 1910–1928.

[24] Chan S T, Leach M J. A validation of FEM3MP with Joint Urban 2003 data. J. Appl. Meteor. Climatol., 2007; 46: 2127–2146.

[25] Hendricks E A, Diehl S R, Burrows D A, Keith R. Evaluation of a fast-running urban dispersion modeling system using joint urban 2003 field data, Appl. Meteor. Climatol., 2007; 46: 2165–2179.

[26] Hanna S, White J, Trolier J, Vernot R, Brown M, Gowardhan A, Kaplane H, Alexander Y, Moussafir J, Wang Y, Williamson C, Hannan J, Hendrick E. Comparisons of JU2003 observations with four diagnostic urban wind flow and Lagrangian particle dispersion models. Atmos. Envi. 2011; 45: 4073-4081.

[27] Nakayama H, Jurcakova K, Nagai H. Large-Eddy Simulation of plume dispersion within various actual urban areas, Adv. Sci. Res. 2010; 10: 33-41.

[28] Skamarock W C, Klemp J B, Dudhia J, Gill D O, Barker D M, Duda M G, Huang X, Wang W, Powers J G. A description of the Advanced Research WRF Version 3, *NCAR Tech. Note*, NCAR/TN-475+STR, 1 pp, 2008.

[29] Janjic Z I. Nonsingular implementation of the Mellor-Yamada level 2.5 scheme in the NCEP Meso model. *NCEP Office Note*, 437, 61 pp, 2002.

[30] COST Action 732, 2005-2009, Quality assurance and improvement of micro-scale meteorological models. http://www.mi.uni-hamburg.de/Official-Documents.5849.0.html.

[31] Gresho P. M. Some interesting issues in incompressible fluid dynamics, both in the continuum and in numerical simulation, Advances in Appl. Mech. 1992; 28: 45–140.

[32] Moeng C H, Sullivan P P. A comparison of shear- and buoyancy-driven planetary boundary layer flows. J. Atmos. Sci. 1994; 51: 999-1022.

[33] Lundquist J K, Chan S T. Consequences of urban stability conditions for computational fluid dynamics simulations of urban dispersion, J. Appl Meteorol. Climatol. 2007; 46: 1080–1097.

[34] Lundquist K A, Chow F K, Lundquist J K. An immersed boundary method enabling large-eddy simulations of flow over complex terrain in the WRF model, Mon. Wea. Rev. 2010; 140, 3936-3955.

[35] Nakayama H, Takemi T, Nagai H. LES analysis of the aerodynamic surface properties for turbulent flows over building arrays with various geometries, J. Appl Meteorol. Climatol. 2011; 6: 79–86.

[36] Davidson M, Mylne K, Jones C, Phillips J, Perkins R, Fung J, Hunt J. Plume dispersion and large groups of obstacles -a field investigation, Atmos. Environ. 1995; 29: 3245-3256.

[37] Michioka T, Sato A, Sada K. Large-eddy simulation for the tracer gas concentration fluctuation in atmospheric boundary layer. Jpn. Soc. Mech. Eng. 2003; B69: 116–123.

[38] Harms F, Leitl B, Schatzmann M, Patnaik G. Validating LES-based flow and dispersion models, J. Wind Eng. Indus. Aerodyn. 2011; 99: 289-295.

Table captions

Table 1 Inflow boundary conditions depending on different mean wind directions.

Table 2 Release conditions during each IOP. CDT indicates Central Daylight Time. The indication *a* means stopped early because of wind shift off sampling grid. Release conditions *C* and *P* indicate puff and 30-minute continuous releases, respectively. Adapted from Allwine and Flaherty [13].

Table 3 Simulation periods for the three plume releases in the LES inner domain.

Table 1. Inflow boundary conditions depending on different mean wind directions.

Case	Mean wind directions	Vertical planes where MM outputs are imposed	Vertical planes where turbulent fluctuations are added
b-1	$-315^\circ \leqq \theta < 0^\circ$ or $0^\circ \leqq \theta < 45^\circ$	West, North, East	North
b-2	$45^\circ \leqq \theta < 135^\circ$	North, East, South	East
b-3	$135^\circ \leqq \theta < 225^\circ$	West, South, East	South
b-4	$225^\circ \leqq \theta < 315^\circ$	North, West, South	West

Table 2. Release conditions during each IOP. CDT indicates Central Daylight Time. The indication *a* means stopped early because of wind shift off sampling grid. Release conditions *C* and *P* indicate puff and 30-minute continuous releases, respectively. Adapted from Allwine and Flaherty [13].

IOP #	Begin Date 2003	Begin/End Time (CDT)	Day/ Night	Release times and conditions
1	6/29	0900/1500	D	8; P, P, P, P, P, P, C, C
2	7/02	0900/1700	D	7; P, P, P, P, C, C, C
3	7/07	0900/1700	D	7; P, P, P, P, C, C, C
4	7/09	0900/1700	D	6; P, P, P, C, C, C
5	7/13	0900/1700	D	7; C, C, C, P, P, P, P
5[a]	7/15	1200/1400	D	3; C, C, C
6	7/16	0900/1700	D	7; C, C, C, P, P, P, P
7	7/18	2300/0700	N	7; C, C, C, P, P, P, P
8	7/24	2300/0700	N	7; C, C, C, P, P, P, P
9	7/26	2300/0700	N	7; C, C, C, P, P, P, P
10	7/28	2100/0400[a]	N	6; C, C, C, P, P, P

Table 3. Simulation periods for the three plume releases in the LES inner domain.

Case		Simulation period	Beginning and ending time of plume release
IOP6	case1	08:00-09:40	09:00-09:30
	case2	10:00-11:40	11:00-11:30
	case3	12:00-13:40	13:00-13:30

Figure captions

Figure 1 Schematic diagram of incorporation meso-scale simulation model outputs into an LES-based CFD model depending on different mean wind directions. The black and dotted lines are computational and main analysis regions, respectively. The open and filled arrows indicate input data of MM outputs and the ones with turbulent fluctuations, respectively.

Figure 2 Locations of meteorological stations used in this study. The meteorological data obtained at the points A, B, and C are compared to those of the WRF and LES models. The photograph is reproduced by Google^{TM} earth graphic.

Figure 3 Locations of concentration measurement in the central business district of Oklahoma City. Time series of concentration fluctuations obtained at the points A-H are compared to those of the LES model. The star mark depicts a point source position which corresponds to the meteorological station B shown in Fig. 1. The photograph is reproduced by Google^{TM} earth graphic.

Figure 4 Computational areas of the WRF and LES models. The WRF is configured with three nested domains covering areas of (a) 2700 km × 2700 km at 4.5 km grid, (b) 600 km × 600 km at 1.5 km grid, and (c) 150 km × 150 km at 500 m grid. The LES model is configured with two nested domains covering areas of (d) 8 km × 8 km at 20m grid and (e) 1.6 km × 1.6 km at 4m grid.

Figure 5 Computational models and mesh arrangement. (a) Driver region for generating urban boundary layer flows by the recycling method. (b) Main analysis region for LESs of plume dispersion in the central business district.

Figure 6 Instantaneous shots of urban boundary layer flows generated from the WRF outputs by the coupling approach and small-scale flows in the urban central district.

Figure 7 Time series of wind speed of observed data (white circles), WRF (thick line), and LES (thin line) at heights of 100 m, 200 m, and 300 m at the point A in the LES outer domain.

~~**Figure 8** Power spectra of wind velocity fluctuations of the LES at heights of 100 m, 200 m, and 300 m at the point A in the LES outer domain.~~

Figure 8 Power spectra of wind velocity fluctuations of the LES for the components of the (a) streamwise and (b) spanwise at heights of 10m, 100 m, 200 m, and 300 m at the point A in the LES outer domain.

Figure 9 Vertical profiles of wind speed at the points A, B, and C at each measuring time for the case1. The results of observed data (white circles), WRF (triangles), and LES (thick line) are indicated. The downstream positions A, B, and C are shown in Fig.2.

Figure 10 Vertical profiles of wind directions at the points A, B, and C at each measuring time for the case1. The indications of each symbol are the same as those in Fig. 7.

Figure 11 The same as Fig.7 except for the case2.

Figure 12 The same as Fig.8 except for the case2.

Figure 13 The same as Fig.7 except for the case3.

Figure 14 The same as Fig.8 except for the case3.

Figure 15 Instantaneous dispersion fields near the ground surface at 8 minutes after the plume release. (a), (b), and (c) indicate the case1, 2, and 3, respectively. The arrow indicates mean wind direction at the point source location. The mean wind directions are 216°, 196°, and 194° for cases1, 2, and 3, respectively. The star mark depicts a point source position.

Figure 16 Time series of concentration fluctuations obtained by the field experiments (black line) and LES model (red line) for the case1. The locations of A-H are shown in Fig. 3.

Figure 17 The same as Fig. 14 except for the case2.

Figure 18 The same as Fig. 14 except for the case3.

Figure 19 Schematic diagram of parameters for statistical study. Adapted from Harms *et al*. [38].

Figure 20 Scatter plot of (a) arrival time, (b) leaving time, (c) duration time, (d) intermittency, (e) averaged concentration, and (f) maximum concentration. The solid line represents perfect agreement. The white circles, triangles, and square indicate the results for the cases1, 2, and 3, respectively.

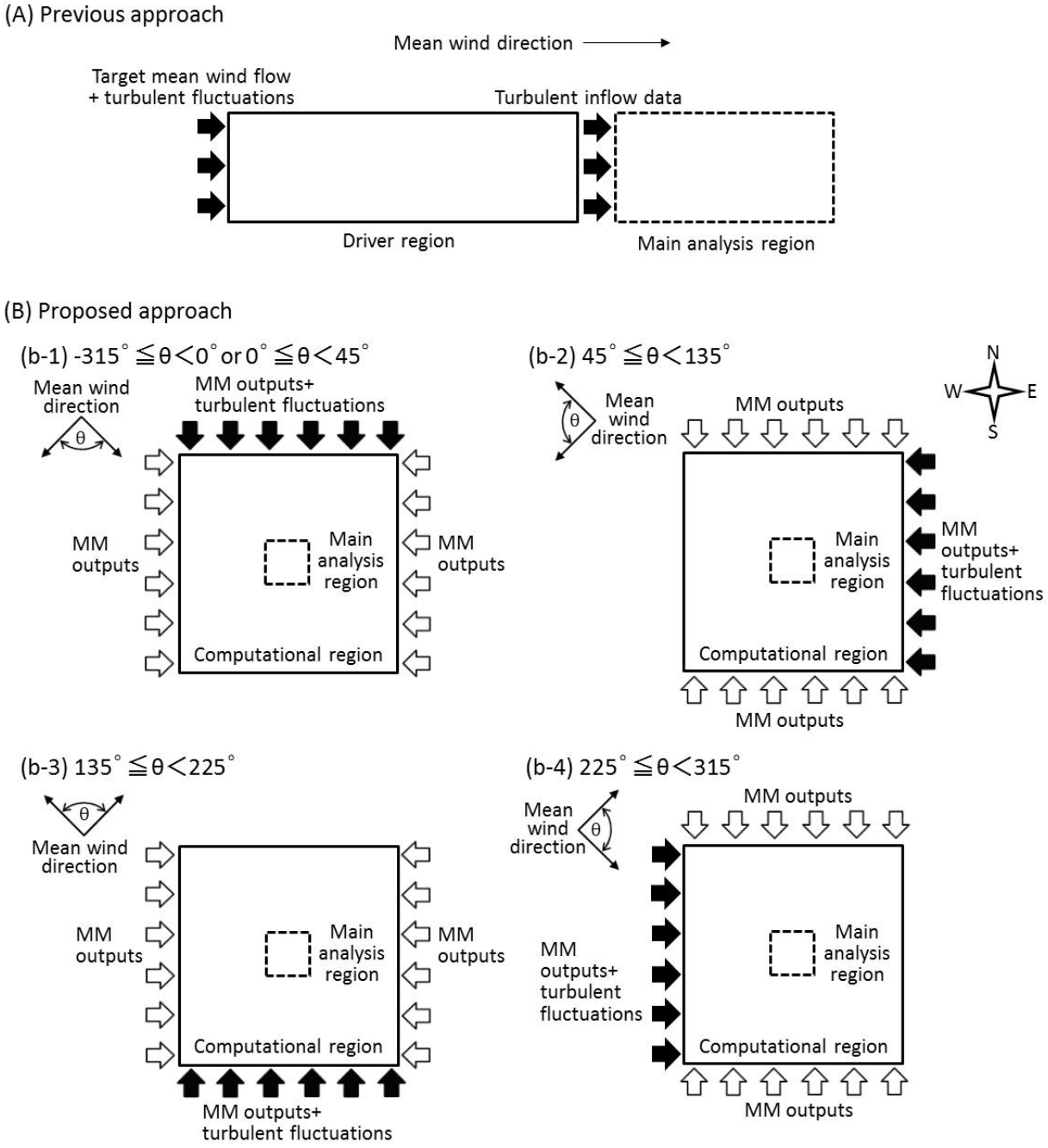

Figure 1. Schematic diagram of incorporation meso-scale simulation model outputs into an LES-based CFD model depending on different mean wind directions. The black and dotted lines are computational and main analysis regions, respectively. The open and filled arrows indicate input data of MM outputs and the ones with turbulent fluctuations, respectively.

H. Nakayama:
Development of Local-Scale High-Resolution Atmospheric Dispersion Model Using Large-Eddy Simulation. Part 5: Detailed Simulation of Turbulent Flows and Plume Dispersion in an Actual Urban Area under Real Meteorological Conditions.

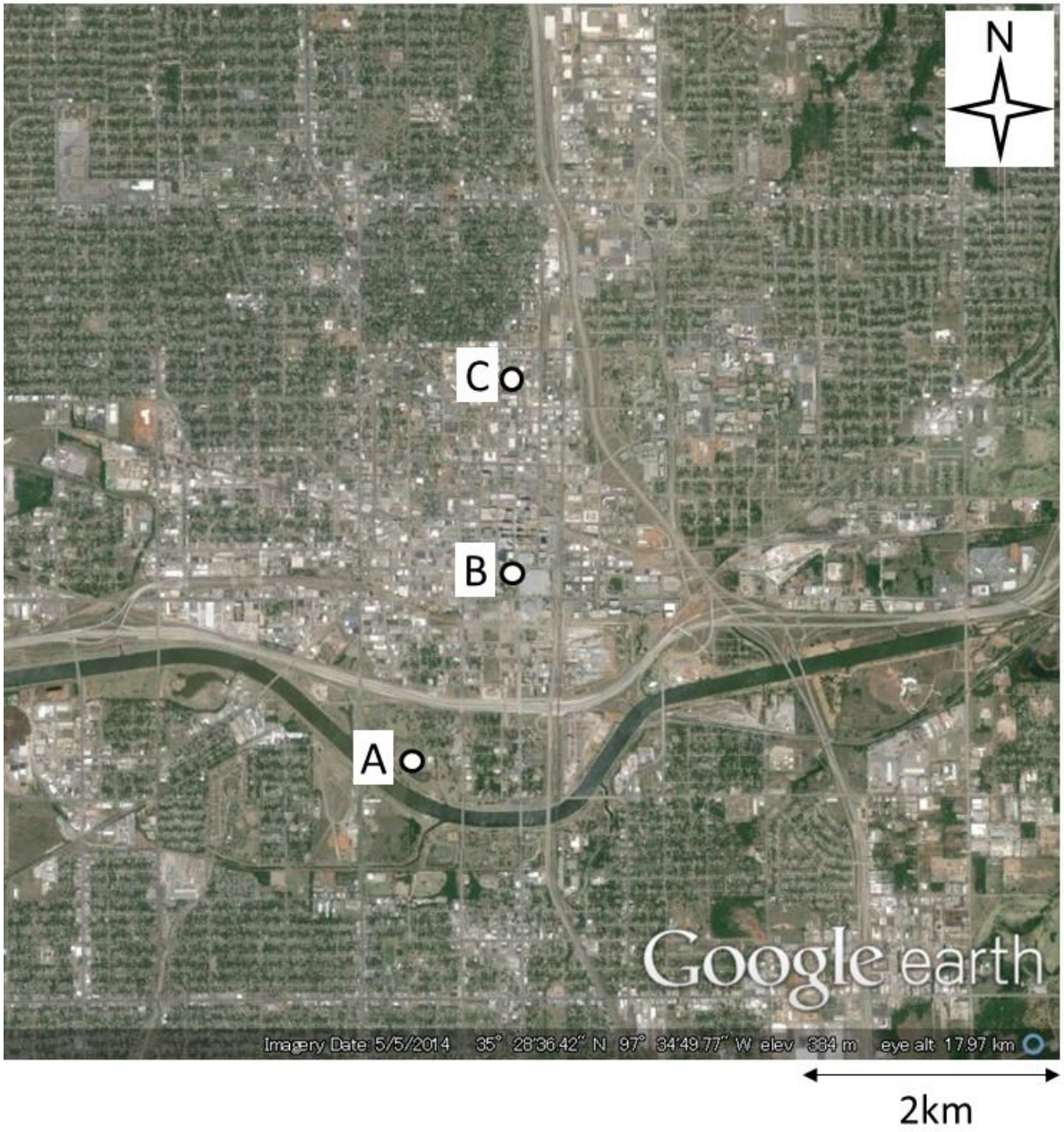

Figure 2. Locations of meteorological stations used in this study. The meteorological data obtained at the points A, B, and C are compared to those of the WRF and LES models. The photograph is reproduced by Google™ earth graphic.

H. Nakayama:

Development of Local-Scale High-Resolution Atmospheric Dispersion Model Using Large-Eddy Simulation. Part 5: Detailed Simulation of Turbulent Flows and Plume Dispersion in an Actual Urban Area under Real Meteorological Conditions.

Color Print

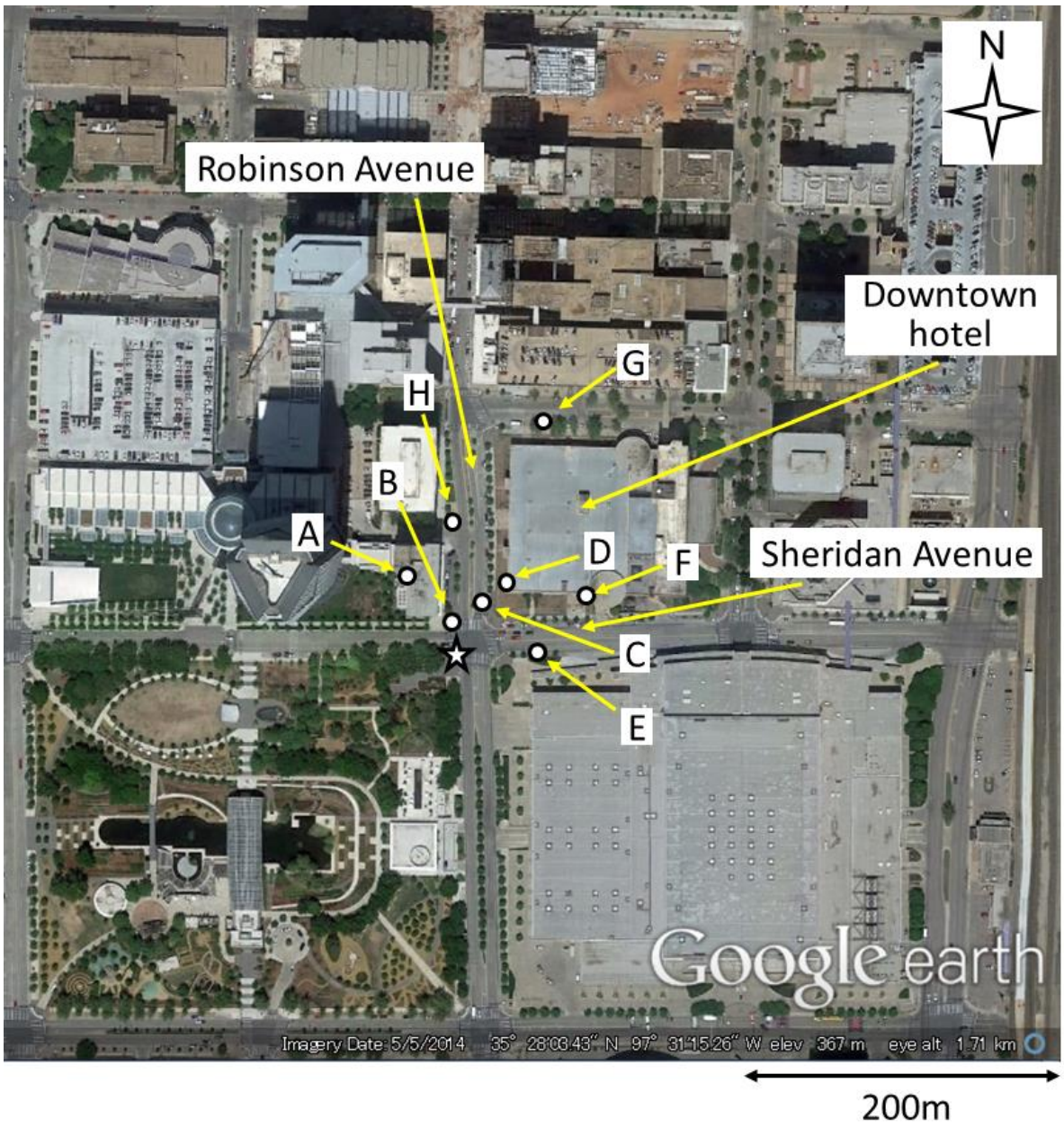

Figure 3. Locations of concentration measurement in the central business district of Oklahoma City. Time series of concentration fluctuations obtained at the points A-H are compared to those of the LES model. The star mark depicts a point source position which corresponds to the meteorological station B shown in Fig. 1. The photograph is reproduced by Google™ earth graphic.

H. Nakayama:
Development of Local-Scale High-Resolution Atmospheric Dispersion Model Using Large-Eddy Simulation. Part 5: Detailed Simulation of Turbulent Flows and Plume Dispersion in an Actual Urban Area under Real Meteorological Conditions.

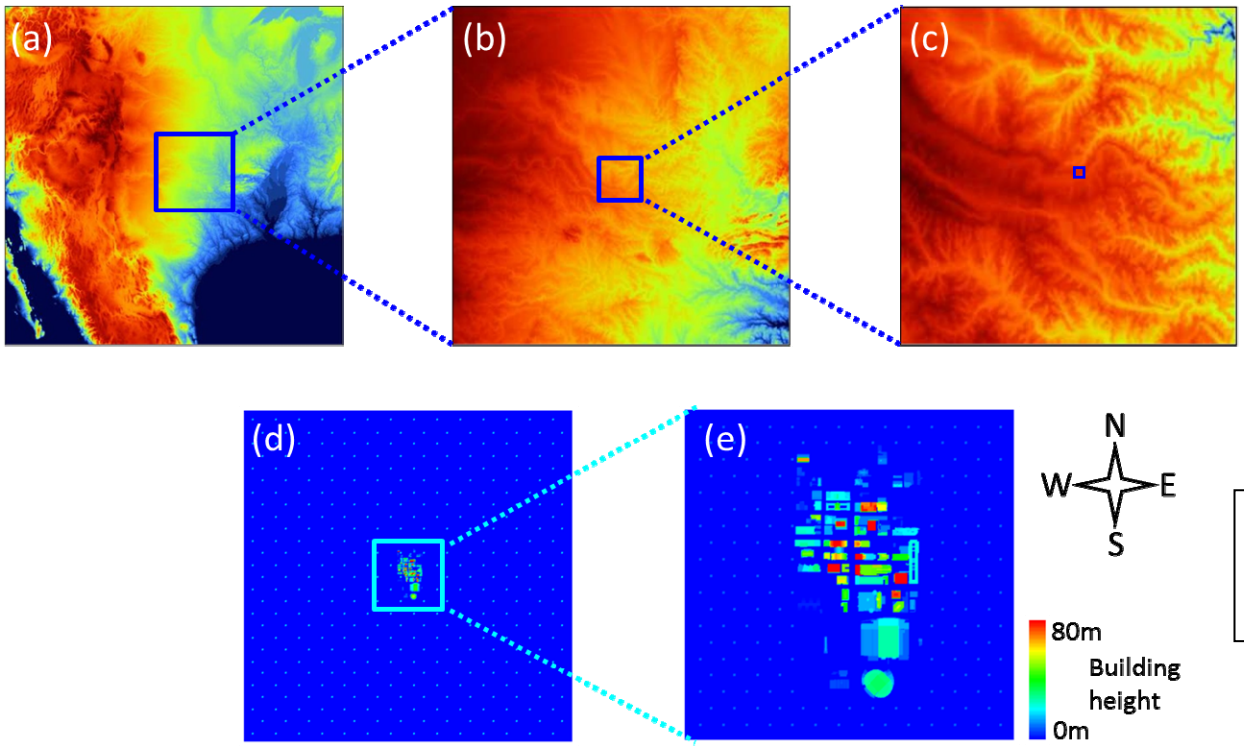

Figure 4. Computational areas of the WRF and LES models. The WRF is configured with three nested domains covering areas of (a) 2700 km × 2700 km at 4.5 km grid, (b) 600 km × 600 km at 1.5 km grid, and (c) 150 km × 150 km at 500 m grid. The LES model is configured with two nested domains covering areas of (d) 8 km × 8 km at 20m grid and (e) 1.6 km × 1.6 km at 4m grid.

H. Nakayama:

Development of Local-Scale High-Resolution Atmospheric Dispersion Model Using Large-Eddy Simulation. Part 5: Detailed Simulation of Turbulent Flows and Plume Dispersion in an Actual Urban Area under Real Meteorological Conditions.

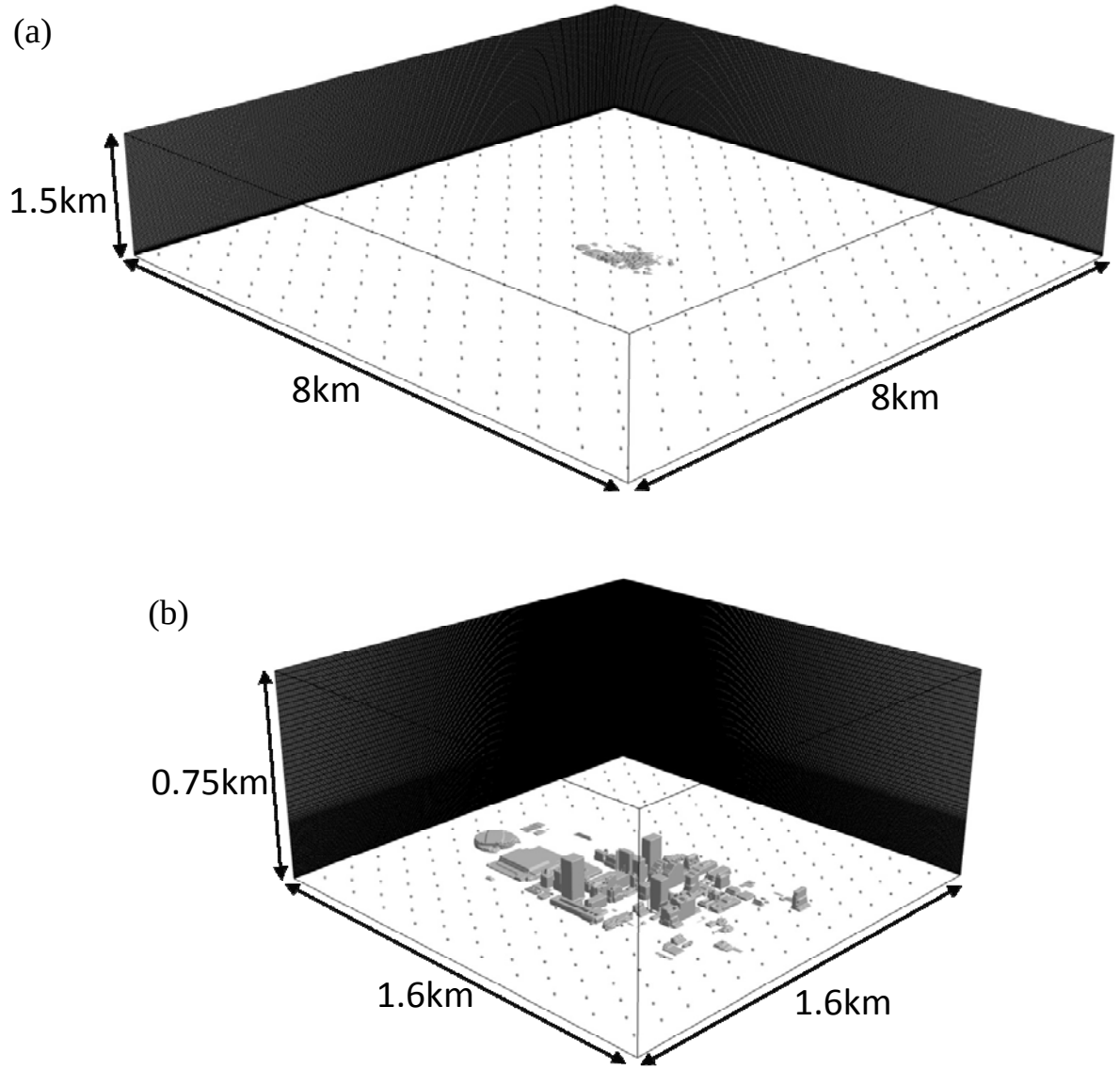

Figure 5. Computational models and mesh arrangement. (a) Driver region for generating urban boundary layer flows by the recycling method. (b) Main analysis region for LESs of plume dispersion in the central business district.

H. Nakayama:

Development of Local-Scale High-Resolution Atmospheric Dispersion Model Using Large-Eddy Simulation. Part 5: Detailed Simulation of Turbulent Flows and Plume Dispersion in an Actual Urban Area under Real Meteorological Conditions.

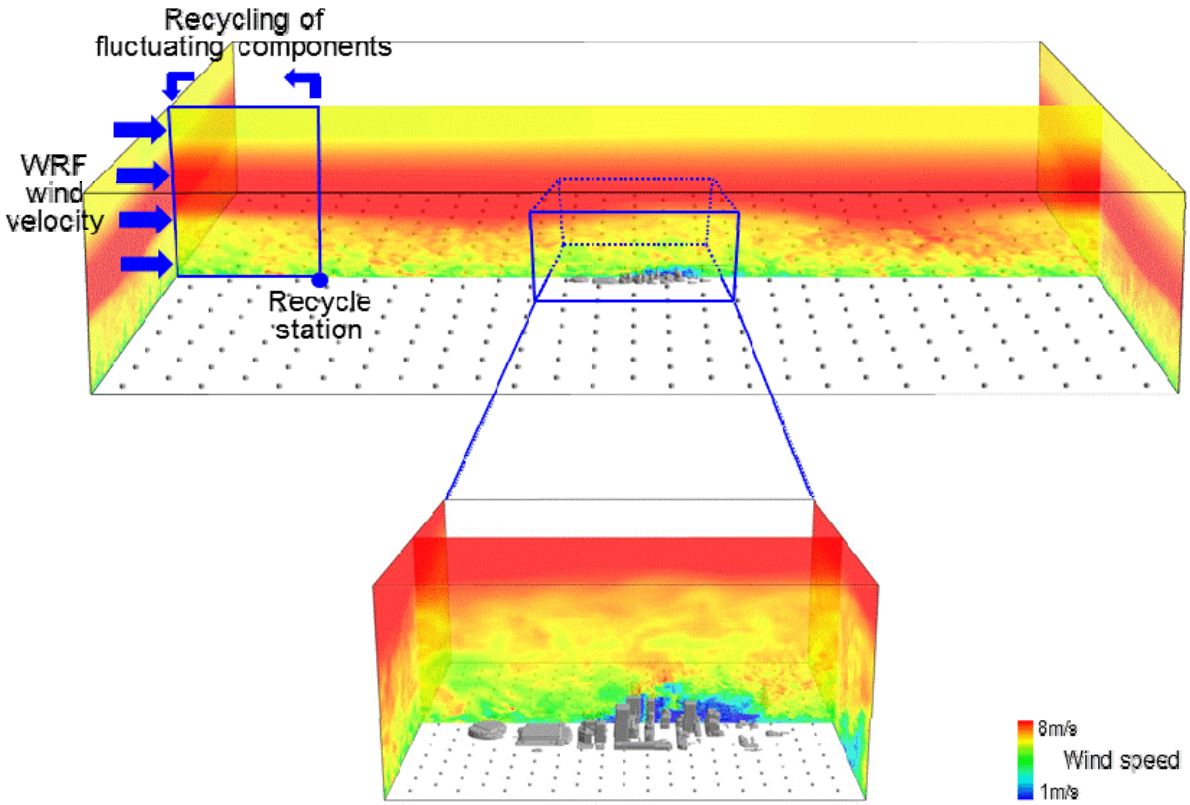

Color Print

Figure 6. Instantaneous shots of urban boundary layer flows generated from the WRF outputs by the coupling approach and small-scale flows in the urban central district.

H. Nakayama:

Development of Local-Scale High-Resolution Atmospheric Dispersion Model Using Large-Eddy Simulation. Part 5: Detailed Simulation of Turbulent Flows and Plume Dispersion in an Actual Urban Area under Real Meteorological Conditions.

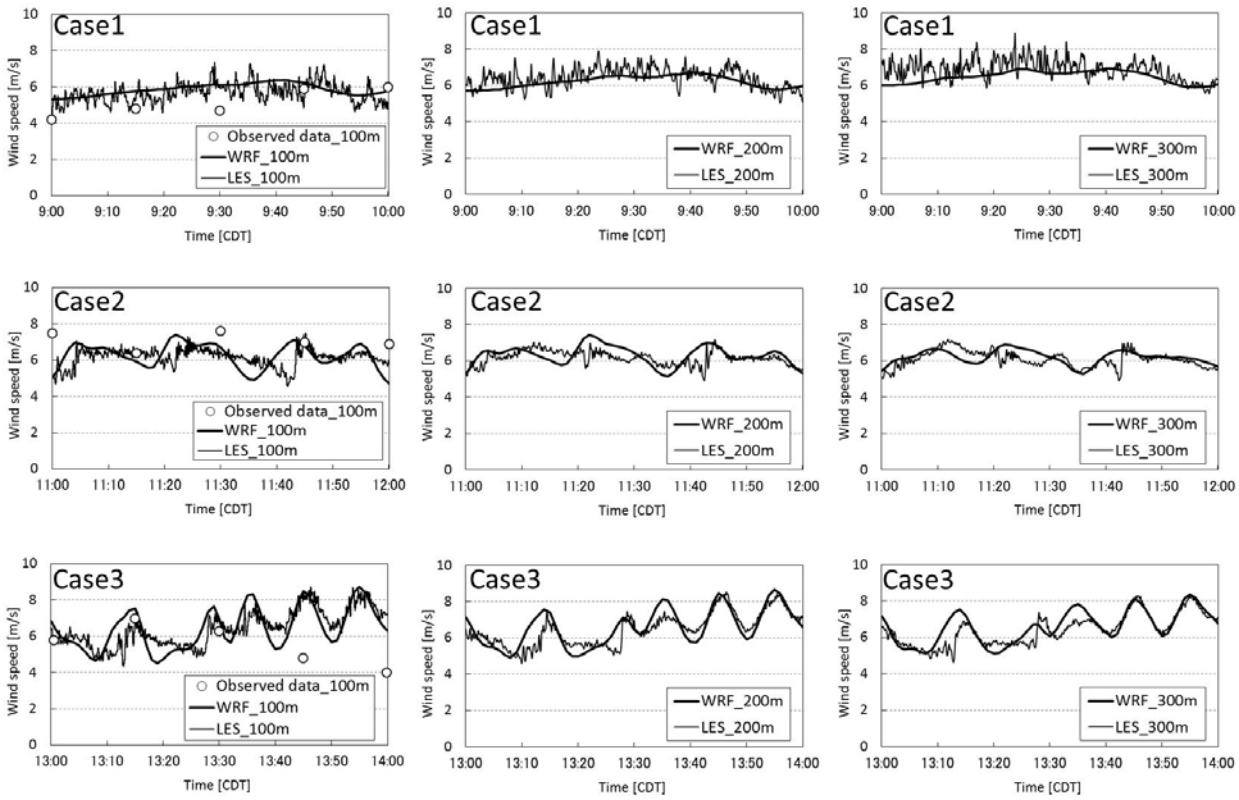

Figure 7. Time series of wind speeds of observed data (white circles), WRF (thick line), and LES (thin line) at heights of 100 m, 200 m, and 300 m at the point A in the LES outer domain.

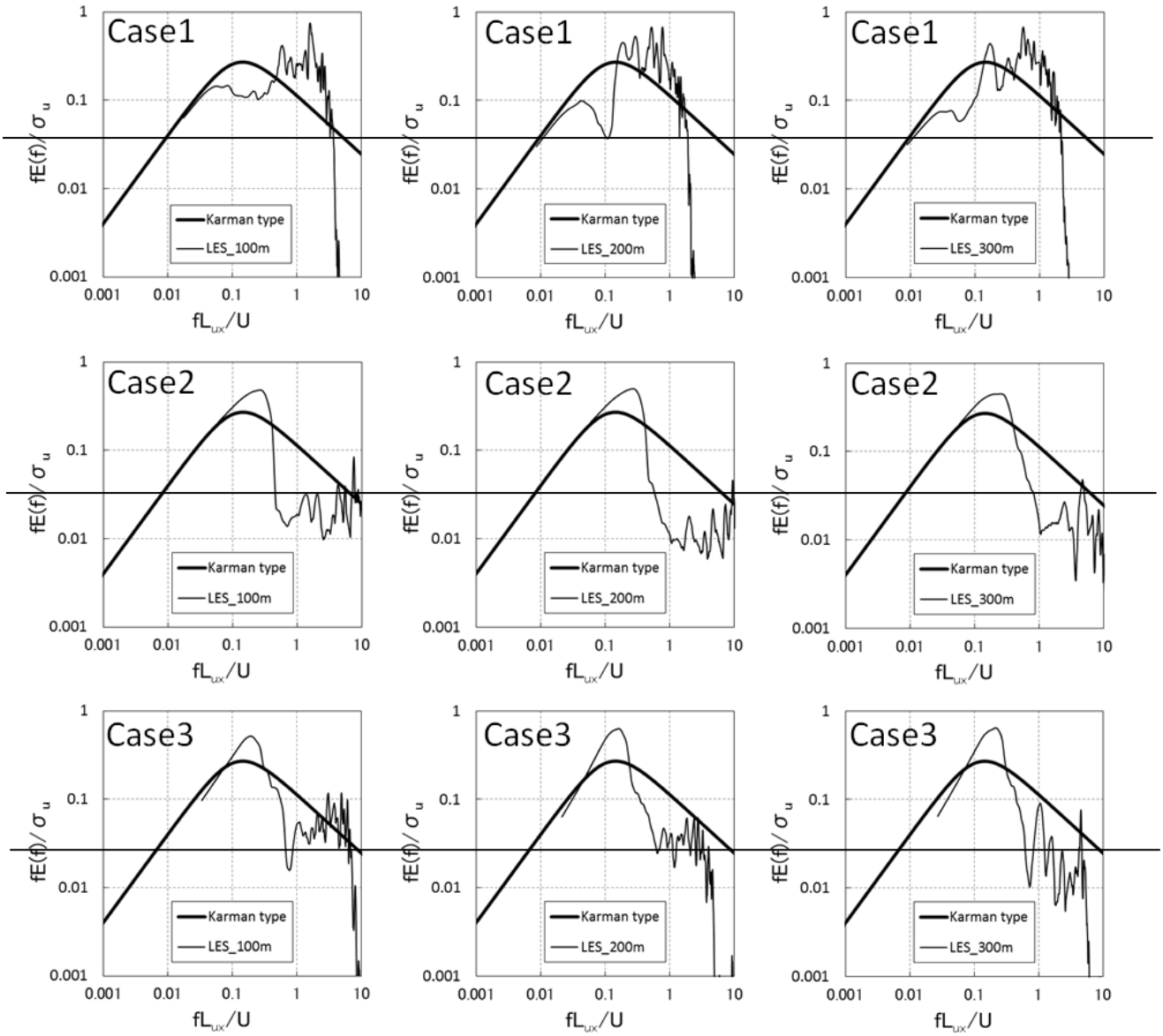

Figure 8. Power spectra of wind velocity fluctuations of the LES at heights of 100 m, 200 m, and 300 m at the point A in the LES outer domain.

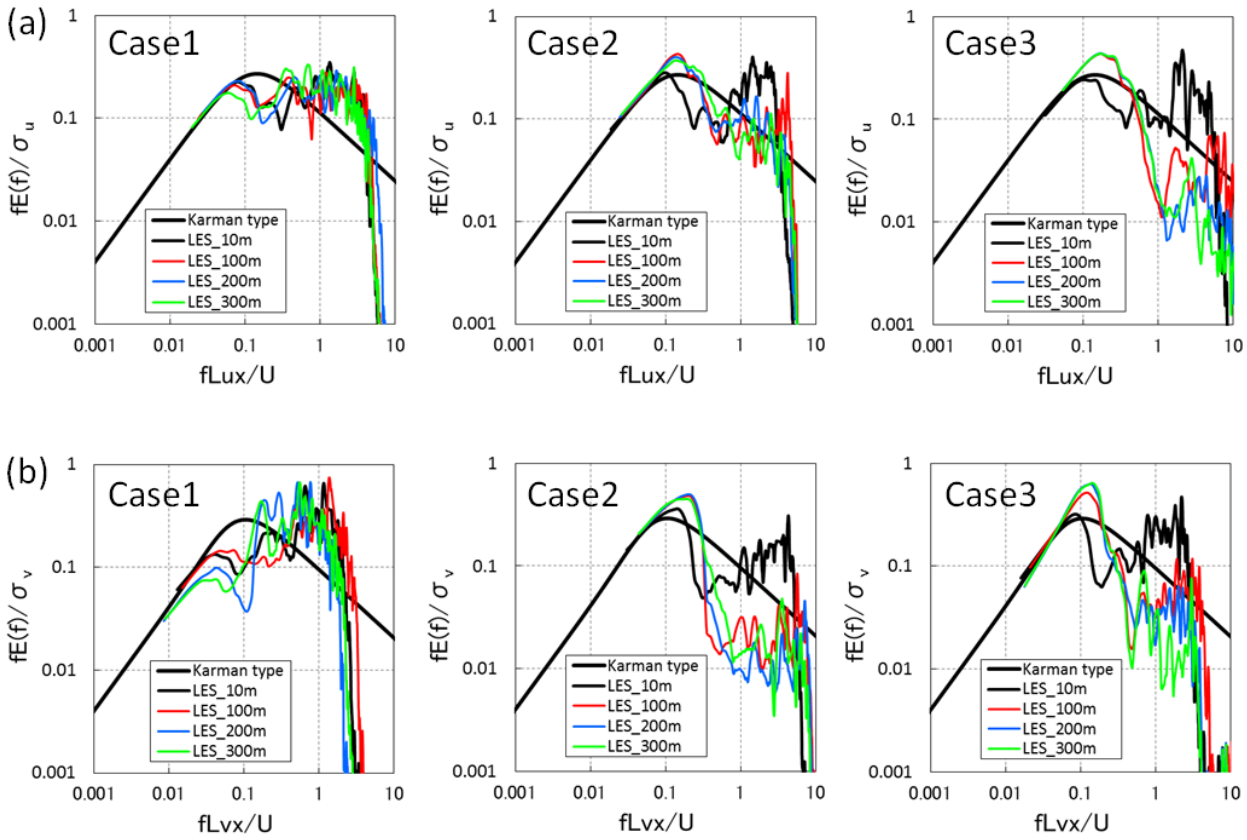

Color Print

Figure 8. Power spectra of wind velocity fluctuations of the LES for the components of the (a) streamwise and (b) spanwise at heights of 10m, 100 m, 200 m, and 300 m at the point A in the LES outer domain.

H. Nakayama:

Development of Local-Scale High-Resolution Atmospheric Dispersion Model Using Large-Eddy Simulation. Part 5: Detailed Simulation of Turbulent Flows and Plume Dispersion in an Actual Urban Area under Real Meteorological Conditions.

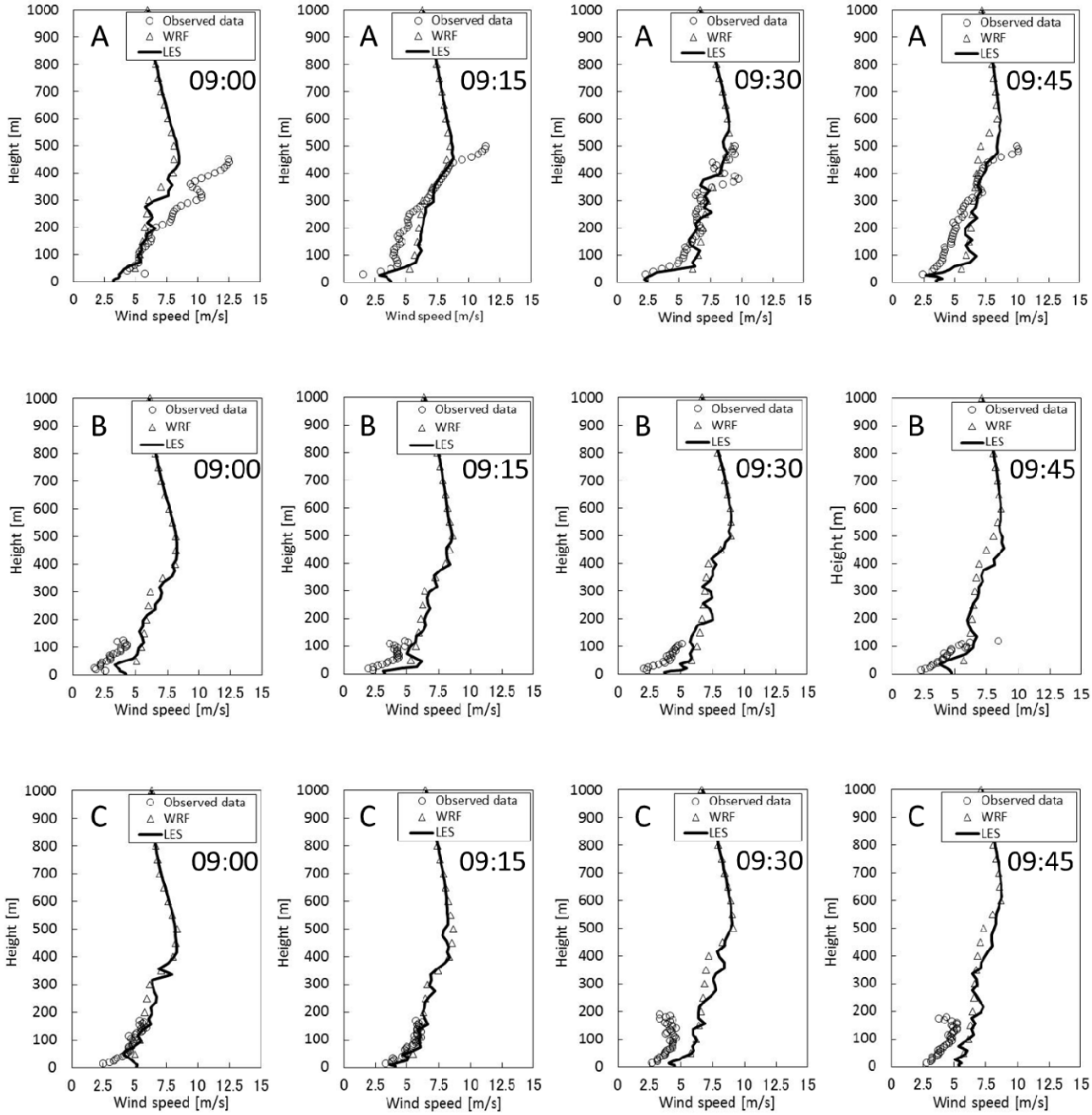

Figure 9. Vertical profiles of wind speed at the points A, B, and C at each measuring time for the case1. The results of observed data (white circles), WRF (triangles), and LES (thick line) are indicated. The downstream positions A, B, and C are shown in Fig.2.

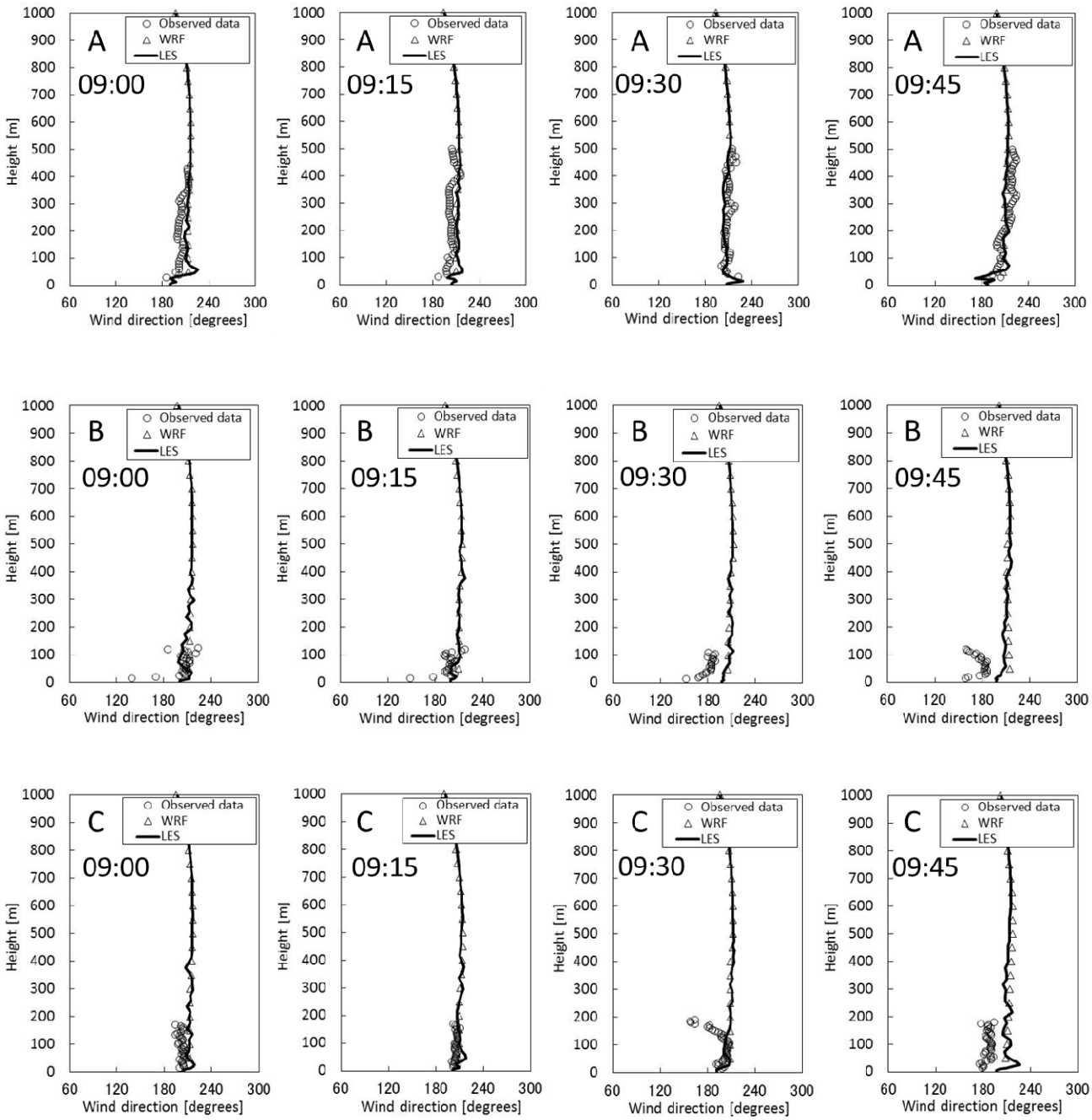

Figure 10. Vertical profiles of wind directions at the points A, B, and C at each measuring time for the case1. The indications of each symbol are the same as those in Fig. 7.

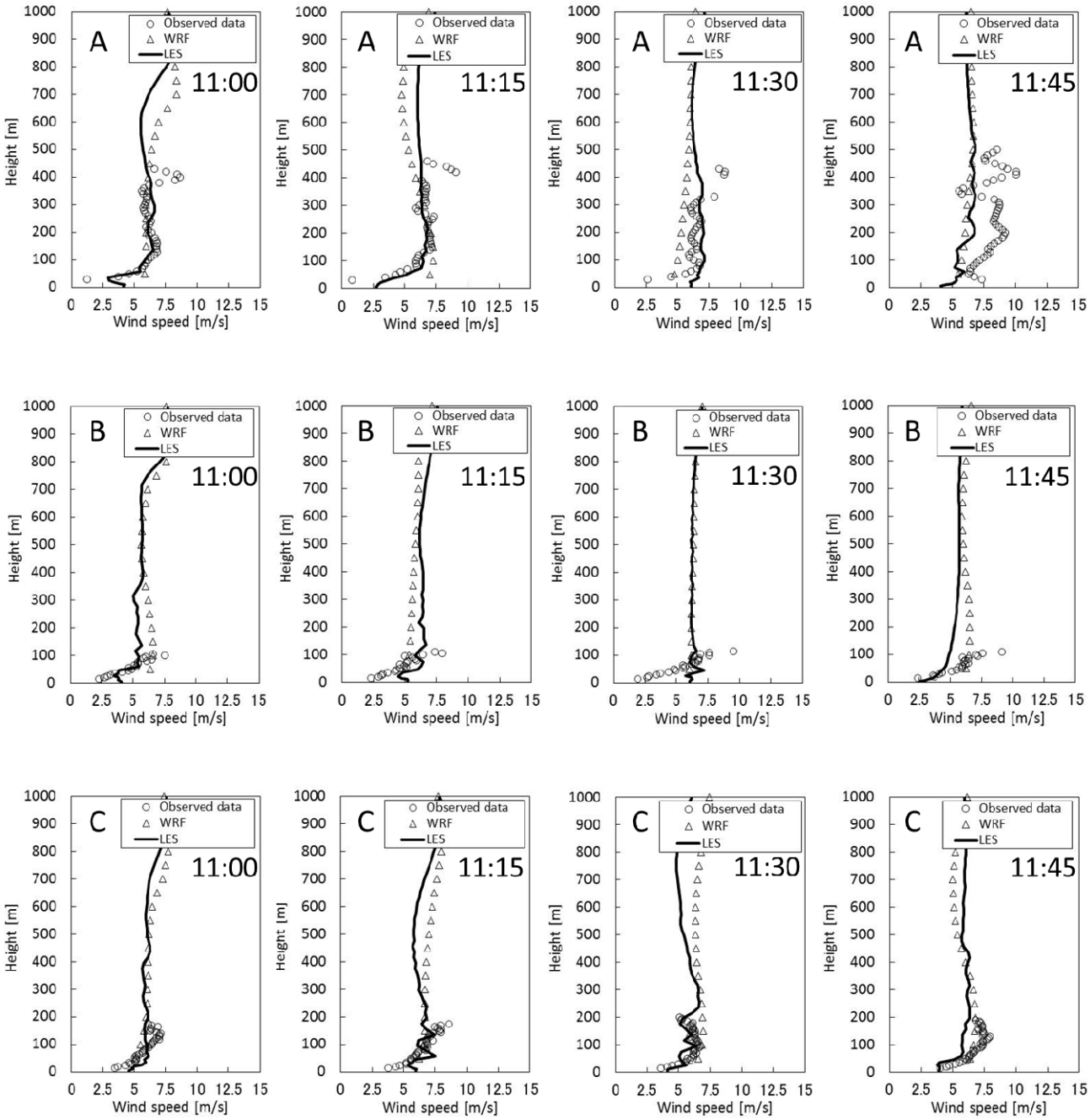

Figure 11. The same as Fig.7 except for the case2.

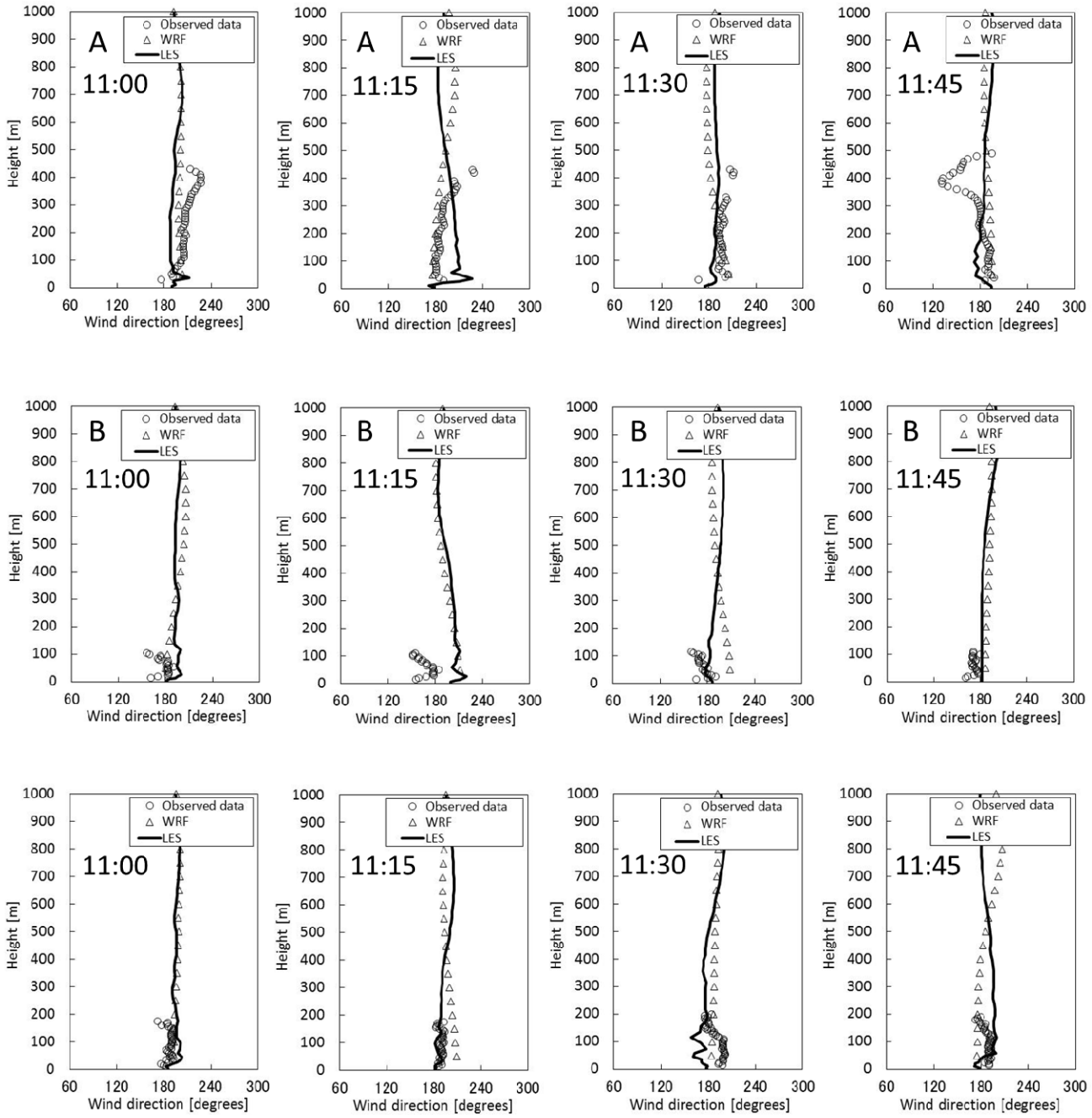

Figure 12. The same as Fig.8 except for the case2.

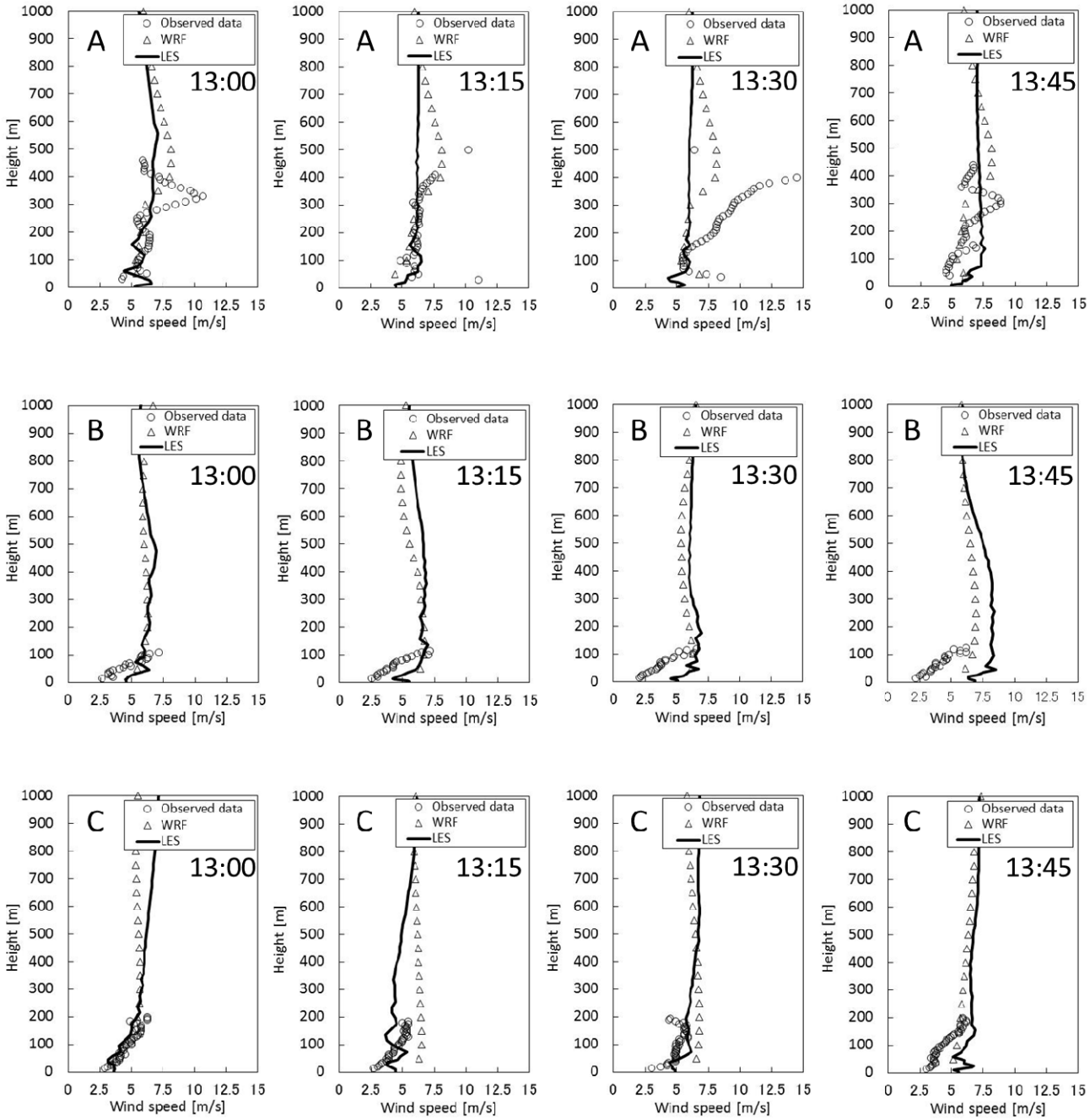

Figure 13. The same as Fig.7 except for the case3.

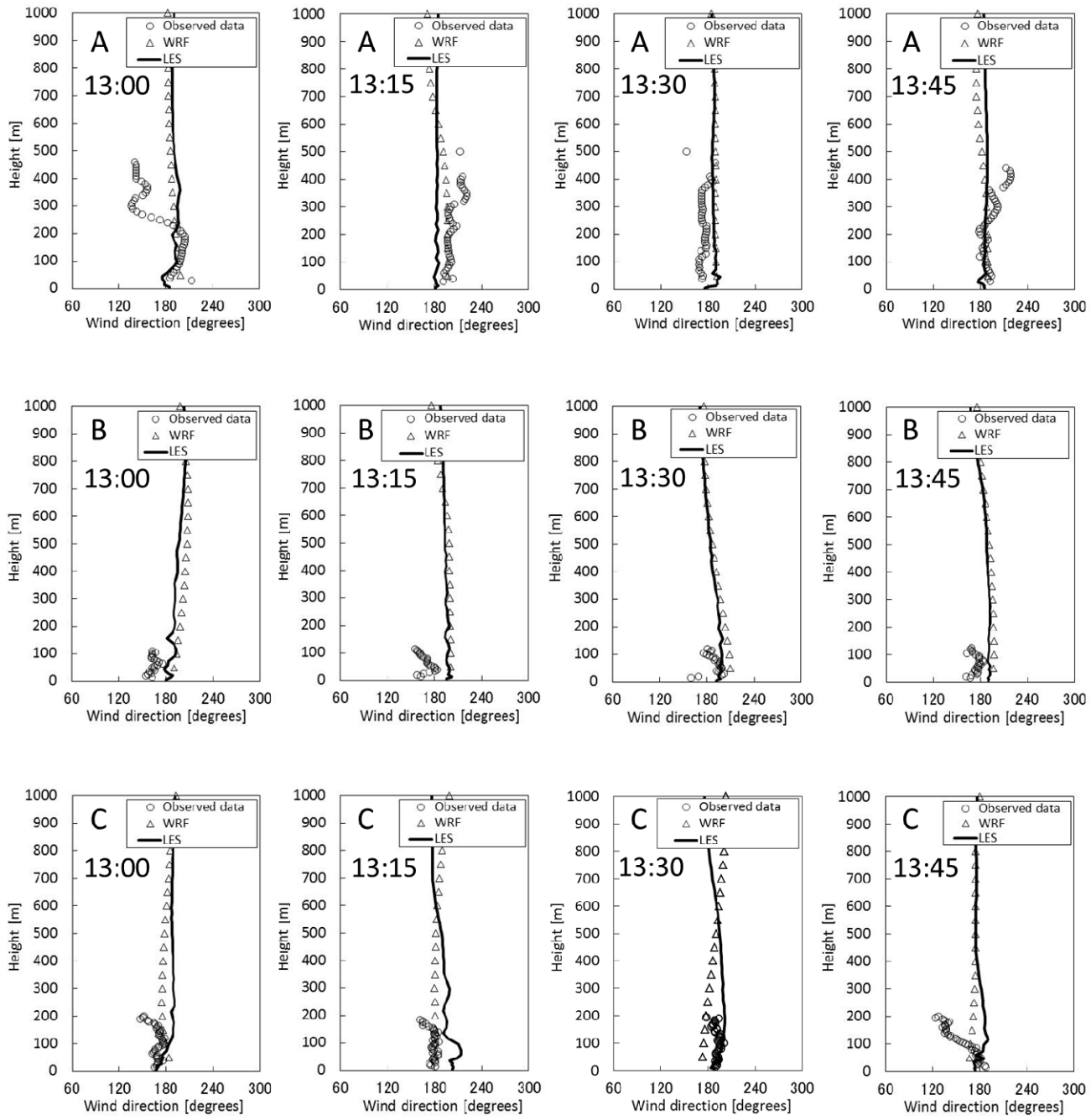

Figure 14. The same as Fig.8 except for the case3.

H. Nakayama:

Development of Local-Scale High-Resolution Atmospheric Dispersion Model Using Large-Eddy Simulation. Part 5: Detailed Simulation of Turbulent Flows and Plume Dispersion in an Actual Urban Area under Real Meteorological Conditions.

Color Print

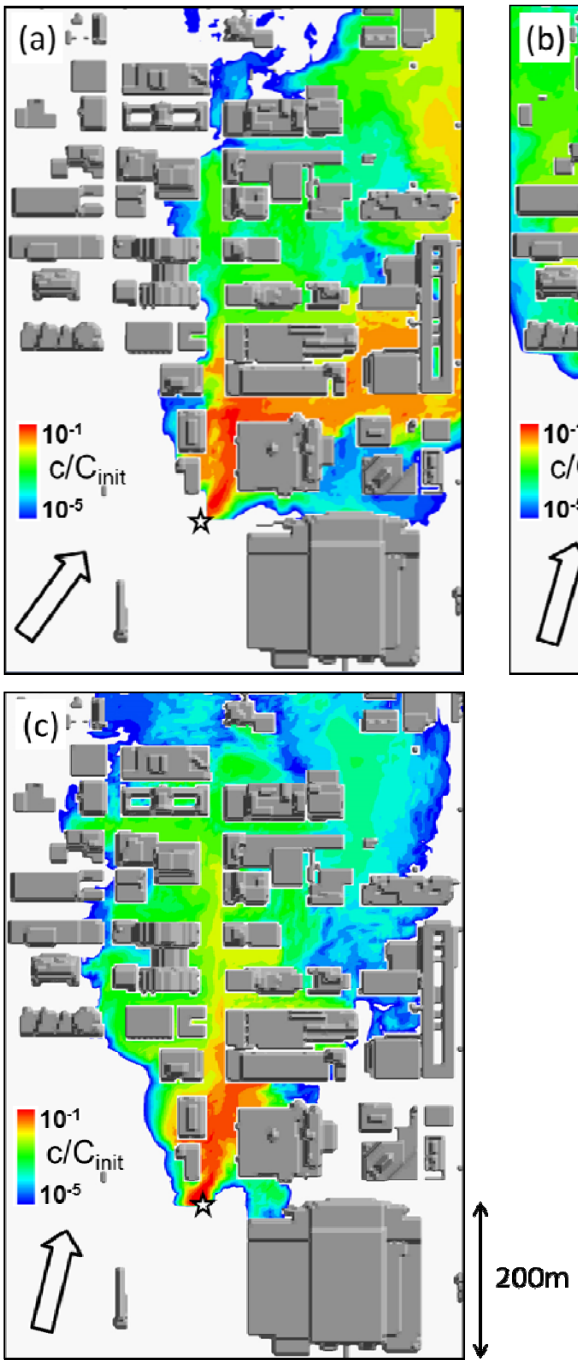

Figure 15. Instantaneous dispersion fields near the ground surface at 8 minutes after the plume release. (a), (b), and (c) indicate the cases1, 2, and 3, respectively. The arrow indicates mean wind direction at the point source location. The mean wind directions are 216°, 196°, and 194° for cases1, 2, and 3, respectively. The star mark depicts a point source position.

H. Nakayama:
Development of Local-Scale High-Resolution Atmospheric Dispersion Model Using Large-Eddy Simulation. Part 5: Detailed Simulation of Turbulent Flows and Plume Dispersion in an Actual Urban Area under Real Meteorological Conditions.

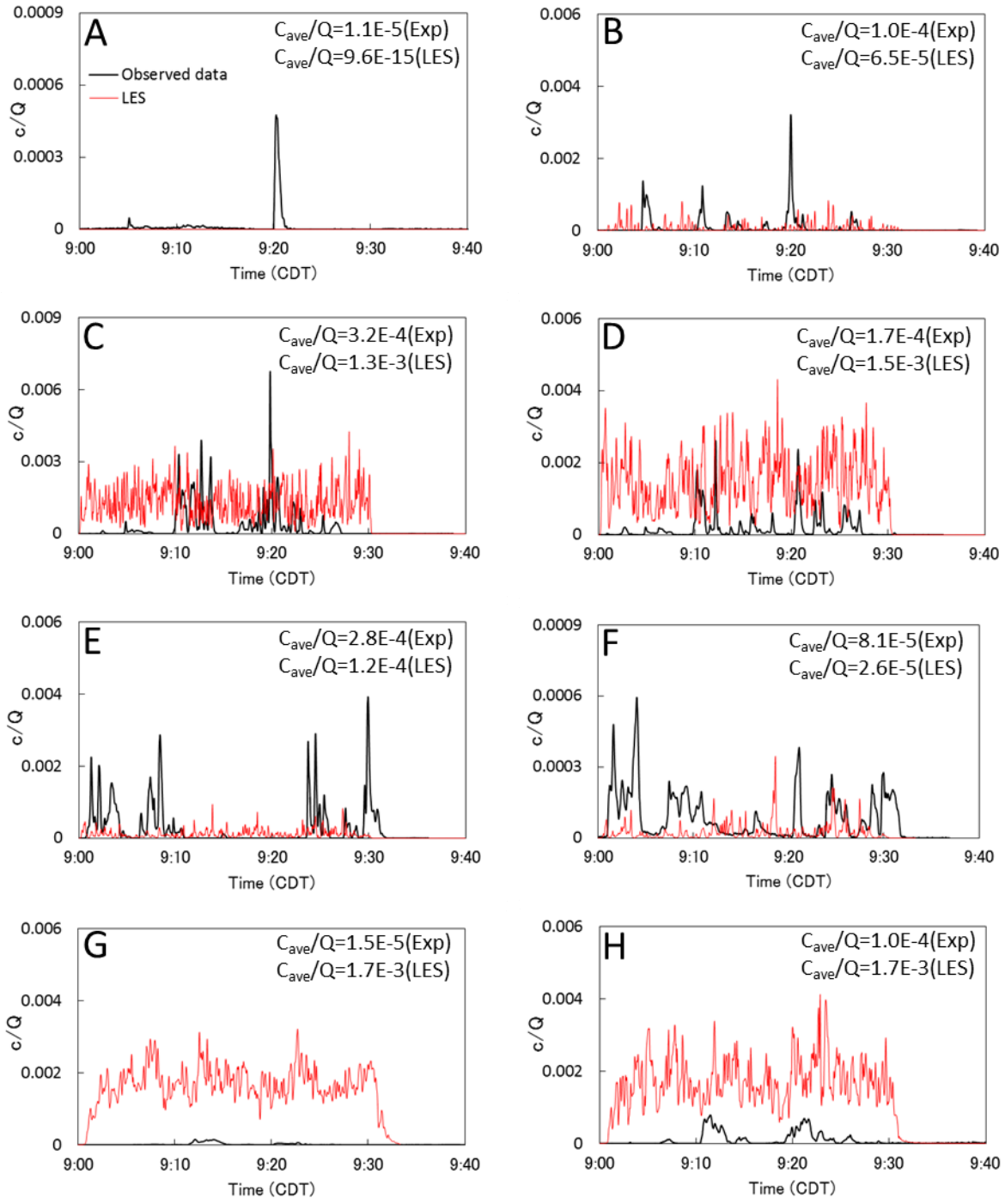

Color Print

Figure 16. Time series of concentration fluctuations obtained by the field experiments (black line) and LES model (red line) for the case1. The locations of A-H are shown in Fig. 3.

H. Nakayama:

Development of Local-Scale High-Resolution Atmospheric Dispersion Model Using Large-Eddy Simulation. Part 5: Detailed Simulation of Turbulent Flows and Plume Dispersion in an Actual Urban Area under Real Meteorological Conditions.

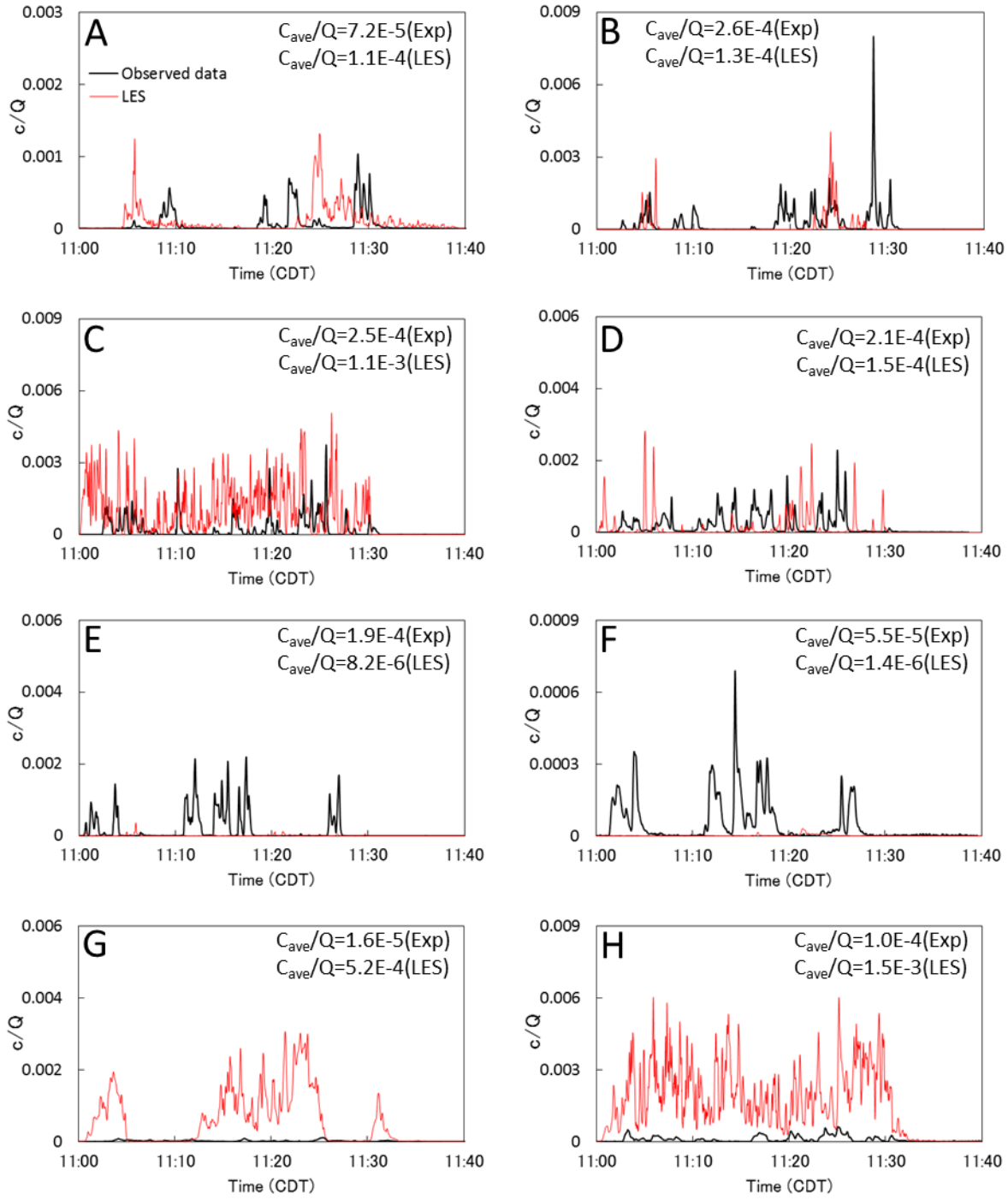

Color Print

Figure 17. The same as Fig. 14 except for the case2.

H. Nakayama:

Development of Local-Scale High-Resolution Atmospheric Dispersion Model Using Large-Eddy Simulation. Part 5: Detailed Simulation of Turbulent Flows and Plume Dispersion in an Actual Urban Area under Real Meteorological Conditions.

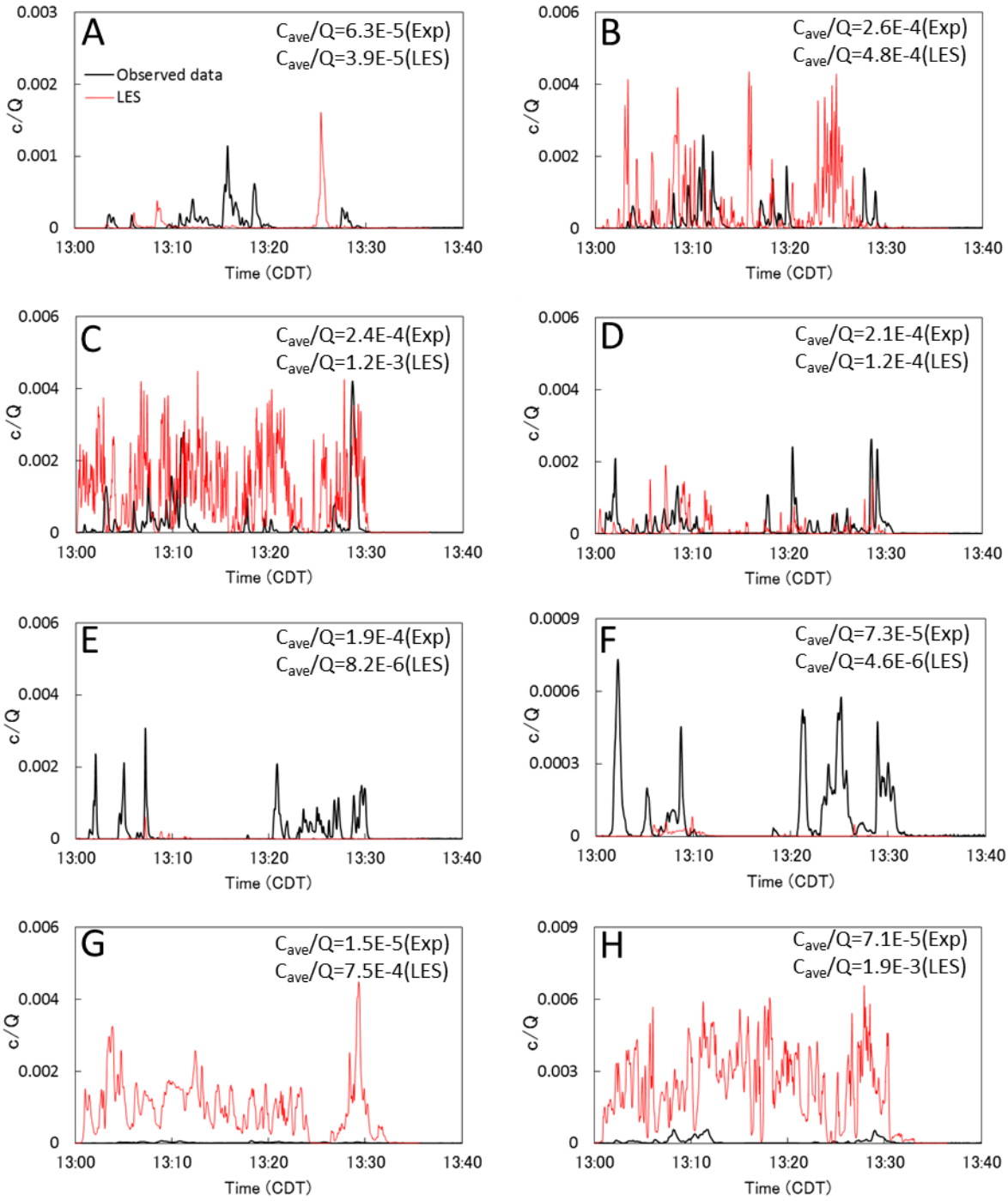

Color Print

Figure 18. The same as Fig. 14 except for the case3.

H. Nakayama:

Development of Local-Scale High-Resolution Atmospheric Dispersion Model Using Large-Eddy Simulation. Part 5: Detailed Simulation of Turbulent Flows and Plume Dispersion in an Actual Urban Area under Real Meteorological Conditions.

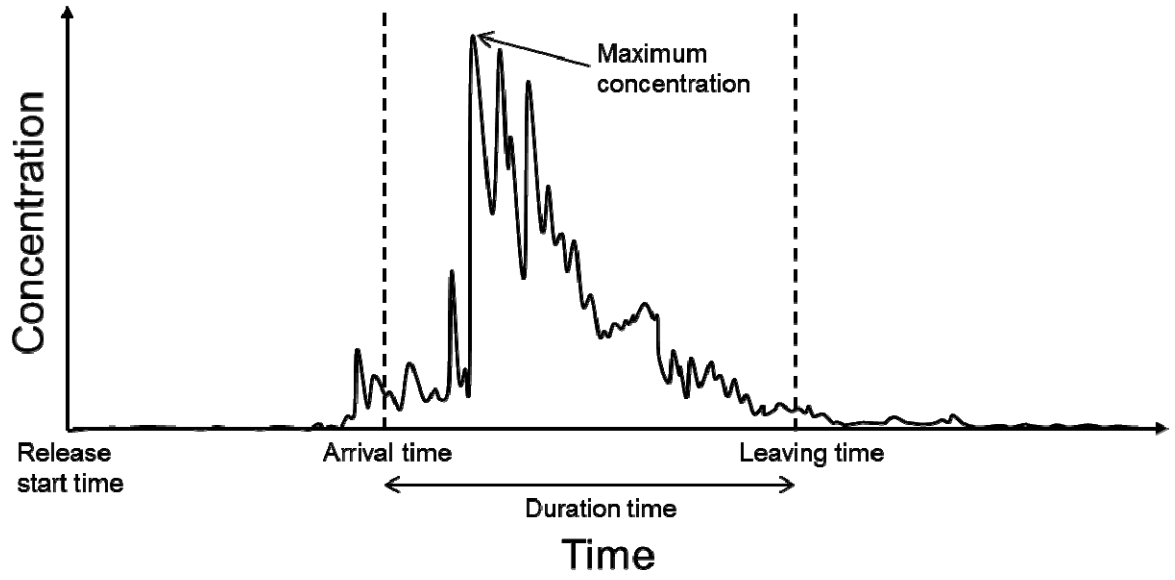

Figure 19. Schematic diagram of parameters for statistical study. Adapted from Harms *et al*. [38].

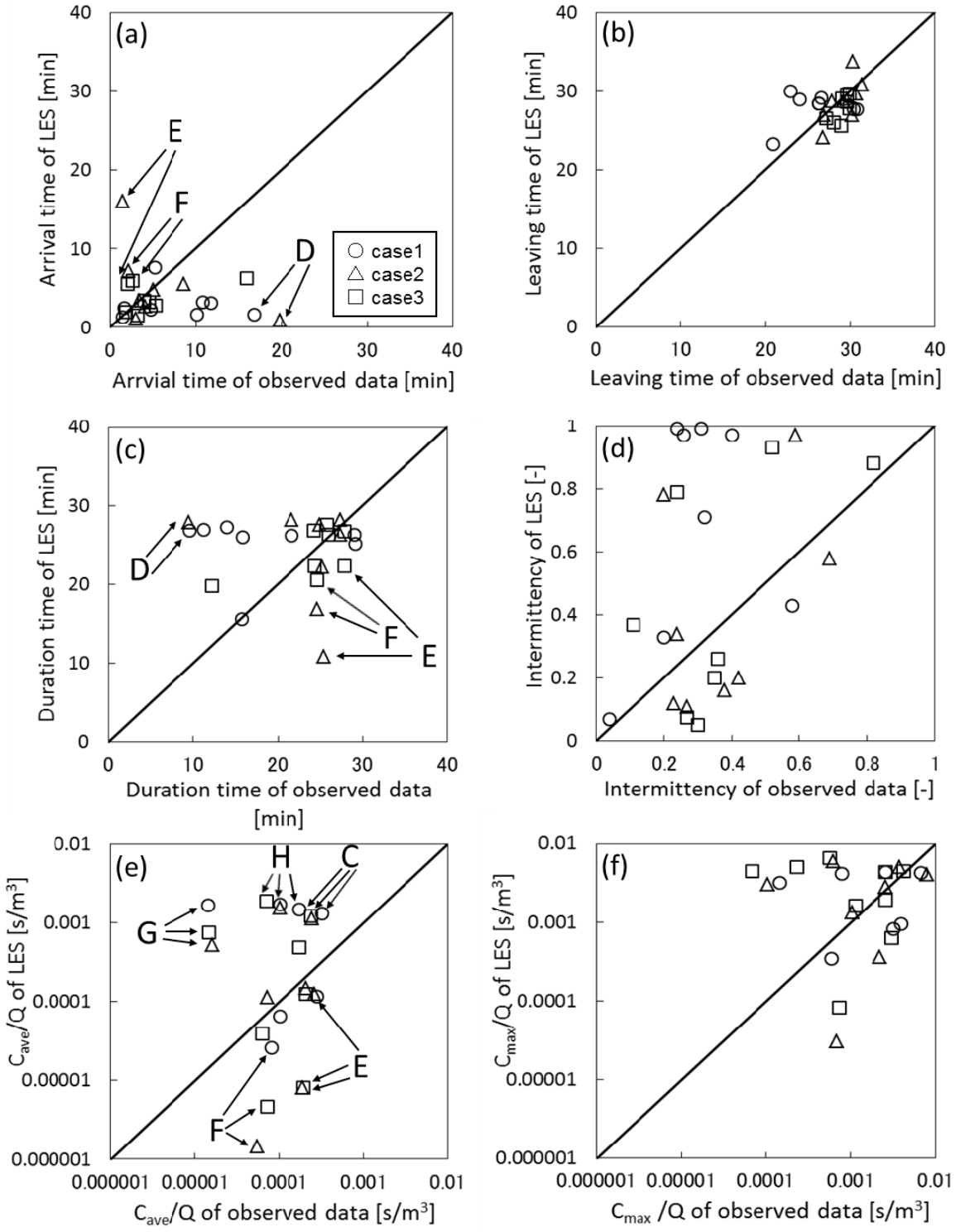

Figure 20. Scatter plot of (a) arrival time, (b) leaving time, (c) duration time, (d) intermittency, (e) averaged concentration, and (f) maximum concentration. The solid line represents perfect agreement. The white circles, triangles, and square indicate the results for the cases1, 2, and 3, respectively.

H. Nakayama:
Development of Local-Scale High-Resolution Atmospheric Dispersion Model Using Large-Eddy Simulation. Part 5: Detailed Simulation of Turbulent Flows and Plume Dispersion in an Actual Urban Area under Real Meteorological Conditions.